TECHNISCHE UNIVERSITÄT WIEN

Energy Economics Group

Master's Thesis

for the achievement of the academic degree

Diplom-Ingenieur

in the field of study Electrical Power Engineering and Sustainable Energy Systems
at TU Wien

Techno-economic assessment of pumped storage hydro power in hybrid operation with floating photovoltaic and battery energy storage

submitted at
Institute of Energy Systems and Electrical Drives

Supervisor (TU Wien): Associate Prof. Dipl.-Ing. Dr.techn. Johann Auer
Assistent (TU Wien): Univ.Ass.in Dipl.-Ing.in Antonia Golab, BSc
Supervisor (AIT): Dipl.-Ing. Sebastian Alexander Steinlechner

by

Andreas Patha
01609934

Vienna, April 2024

Abstract

This thesis investigates the techno-economic impact of a floating PV system (FPV) and a battery energy storage system (BESS) in hybrid operation with pumped storage hydro power plants (PSHP) traded on the day-ahead market. It is assumed that FPV brings additional benefits to the PSHP by reducing evaporation and thus increasing the overall efficiency of the storage. Other advantages, such as sharing the grid connection and increasing the utilization of FPV generation by reducing curtailment, are also evaluated. A comparison is made between the binary and ternary operation of the PSHP, in which the ternary mode of operation increases operational flexibility. An existing storage power plant in central Sweden, for which Global Hydro provides specific data, is used as a reference for the PSHP. A steady-state simulation is used, which is optimized for trading on the day-ahead market. The simulation framework used for the technical model is the internal TESCA framework of the Austrian Institute of Technology (AIT), which is a Python-based tool for the techno-economic assessment of different technologies. The optimization model is a linearized abstraction implemented with the Julia-based optimization tool IESOpt of the AIT. The simulation is performed for different quantities of nominal FPV power, battery usable energy capacity and BESS storage duration (ratio of usable energy capacity and maximum discharge/charge power) within a parameter study to show the impact on the technical and economic key performance indicators. The levelized cost of energy (LCOE) and net present value (NPV) of the entire hybrid system are calculated for different weighted average costs of capital to assess the economic viability of the entire hybrid system. It is shown that the combined operation of FPV and PSHP can make better use of the limited grid connection capacity, as the FPV electricity can serve as input for the pumps. The BESS adds further storage capacity to store FPV generation and shift it via arbitrage to times of high energy prices. Overall, FPV and BESS increase the LCOE as the additional costs are not compensated by the energy surplus. The NPV is reduced by both technologies and makes the entire system economically nonviable for increasing nominal FPV power and BESS usable energy capacity.

Kurzfassung

In dieser Arbeit werden die technisch-wirtschaftlichen Auswirkungen einer schwimmenden PV-Anlage (FPV) und eines Batteriespeichersystems (BESS) im Hybridbetrieb mit Pumpspeicher-Wasserkraftwerken (PSHP) untersucht, die auf dem Day-Ahead-Markt gehandelt werden. Es wird davon ausgegangen, dass die FPV dem PSHP zusätzliche Vorteile bringt, indem sie die Verdunstung reduziert und somit die Gesamteffizienz des Speichers erhöht. Weitere Vorteile, wie die gemeinsame Nutzung des Netzanschlusses und die Erhöhung der Auslastung der FPV-Erzeugung durch Verringerung der Abregelung, werden ebenfalls bewertet. Es wird ein Vergleich zwischen binärem und ternärem Betrieb des PSHP gezogen, bei dem der ternäre Betrieb die betriebliche Flexibilität erhöht. Für das PSHP wird ein bestehendes Speicherkraftwerk in Mittelschweden als Referenz genommen, für das Global Hydro spezifische Daten zur Verfügung stellt. Es wird eine stationäre Simulation angewendet, die für den Handel auf dem Day-Ahead-Markt optimiert ist. Als Simulationsframework für das technische Modell wird das interne TESCA-Framework des Austrian Institute of Technology (AIT) verwendet, welches ein Python-basiertes Tool zur techno-ökonomischen Bewertung verschiedener Technologien ist. Das Optimierungsmodell ist eine linearisierte Abstraktion, die mit dem Julia-basierten Optimierungstool IESOpt des AIT implementiert wurde. Die Simulation wird für verschiedene Größen der nominalen FPV-Leistung, der nutzbaren Energiekapazität der Batterie und der BESS-Speicherdauer (Verhältnis von nutzbarer Energiekapazität und maximaler Entlade-/Ladeleistung) innerhalb einer Parameterstudie durchgeführt, um den Einfluss auf die technischen und wirtschaftlichen Leistungsindikatoren zu zeigen. Die Stromgestehungskosten (LCOE) und der Kapitalwert (NPV) des gesamten Hybridsystems werden für verschiedene gewichtete durchschnittliche Kapitalkosten berechnet, um die wirtschaftliche Rentabilität zu bewerten. Es zeigt sich, dass durch den kombinierten Betrieb von FPV und PSHP die begrenzte Netzanschlusskapazität besser genutzt werden kann, da der FPV-Strom als Input für die Pumpen dienen kann. Das BESS fügt eine weitere Speicherkapazität hinzu, um die FPV-Erzeugung zu speichern und sie über Arbitrage auf Zeiten hoher Energiepreise zu verlagern. Insgesamt erhöhen FPV und BESS die LCOE, da die zusätzlichen Kosten nicht durch den Energieüberschuss kompensiert werden. Der Kapitalwert wird durch beide Technologien verringert und macht das gesamte System wirtschaftlich unrentabel, wenn die Nennleistung des FPV und die nutzbare Energiekapazität des BESS erhöht werden.

Contents

List of abbreviations

AIT	Austrian Institute of Technology
HPP	Hybrid power plant
PV	Photovoltaic
FPV	Floating photovoltaic
MPP	Maximum power point
E	Evaporation
PSHP	Pumped storage hydro power
A	Area
V	Volume
$\mathbf{h_{loss}}$	Loss head
$\mathbf{h_{act}}$	Actual geodetic head
$\mathbf{h_{eff}}$	Effective head
k	Equivalent sand roughness
L	Length
D	Diameter
Q	Flow
ρ	Density
g	Gravity
Re	Reynolds number
η	Efficiency
P	Power
BESS	Battery energy storage system
SOC	State of charge
DOD	Depth of discharge
KPI	Key performance indicator
FLH	Full load hours
LCOE	Levelized costs of electricity
NPV	Net present value
CAPEX	Capital expenditures
OPEX	Operational expenditures
WACC	Weighted average costs of capital
$\mathbf{C_{el}}$	Electricity costs
$\mathbf{R_{el}}$	Revenues
EUR	Euro
SEK	Swedish Kronor

1 Introduction

1.1 Motivation

Climate change and the associated rise in the global average temperature are a major challenge for humanity. In order to drastically reduce the rise in temperature, the energy supply must be completely decarbonized, which requires a switch to 100% renewable energy generation. In their Net Zero by 2050 study [1] the International Energy Agency states, that the worldwide electricity demand will increase by 40% by the year 2030 and even more than two and a half times by 2050 to reach net zero CO_2 emissions by 2050. Therefore, global generation from renewables has to nearly triple by 2030 and grow eightfold by 2050 for which wind turbines and PV will be the main generation technologies by generating almost 35% of all electricity demand each. Pairing battery energy storage systems (BESS) with solar PV and wind to improve power system flexibility and maintain electricity security becomes commonplace in the late 2020s, complemented by demand response for short duration flexibility and hydro power for flexibility across days or even seasons. [1]

For this increase in PV expansion capacity, not only land- or building-based solutions need to be considered, but all possible solutions need to be taken into account. Reservoirs of (pumped) storage power plants can serve as installation sites for a floating PV system (FPV). This hybrid operation can have advantages as it allows the storage of FPV generation that would be curtailed from a technical point of view or arbitrates it to times of high market prices. In addition, the FPV serves as a cover for the water and thus enables a reduction in evaporation, which has already been a problem in areas with high temperatures and will increase drastically in the future due to rising temperatures. [2]

1.2 Research questions

This thesis aims to provide an initial insight into the field of hybrid pumped storage hydro power plants (PSHP) in cooperation with an FPV system and a BESS. For this purpose, the operation is optimized for trading on the day-ahead market and simulated

via a steady-state simulation. Insights into the hybridization potential will be provided by a techno-economic evaluation of the entire hybrid PSHP by analyzing the influence of increasing sizes of FPV and BESS with a parameter study.

As already mentioned, another advantage of the FPV is the lower evaporation due to covering the water surface by the floats. This is also evaluated in this work by implementing a regression model to reduce evaporation in the simulation.

In PSHP, water can be turbined for generation and pumped to fill the storage reservoir in times of low energy prices. In contrast to the wide range of operation of turbines, pumps with synchronous generators without inverters have a fixed electrical power setpoint for a specific head, as they are driven directly from the power grid. To make pump operation more flexible, it is possible to drive the pump with this invariable electrical power and divert part of the resulting flow rate to the turbine. The turbine can then generate electricity flexibly, which reduces the total amount of electricity drawn from the grid. This means that the grid withdrawal can be controlled more flexibly than with pure pump operation. This operation is referred to as a ternary operation. To compare binary (either pump or turbine are in operation) and ternary operation, these are also compared in this thesis.

The research questions to be answered in this paper therefore are:

- What are the quantitative implications, both in terms of technical functionality and economic viability, of integrating FPV systems and BESS within the framework of PSHP?
- What is the influence of FPV installations on PSHP reservoir evaporation rates?
- What is the significance of ternary operation in PSHP?

1.3 Outline of the thesis

In Section 2 a literature review is offered covering both the BESS and FPV, where on the one hand a technological overview is given and on the other hand benefits in combined operation with PSHP are briefly discussed. Section 3 presents the methodology applied to assess the technical and economic viability and the results stated in the research questions. The simulation process used in the work is discussed, while the economic performance indicators (KPIs) based on the technical results are then described. Finally, the input data required for the simulation and evaluation are addressed. In Section 4 the results of the technical simulation and economic evaluation are presented and discussed based on which the conclusions are drawn in Section 5.

2 Literature review

2.1 Battery energy storage systems

Batteries have a wide field of operation applications which range from ancillary services for the grid to market-driven usage and effectively also combinations of the above [3]. This Section shall give a short overview of the commonly used applications of battery operation based on [3].

- **Peak shaving:** The demand throughout a day varies and is therefore not uniform. To get a smoother profile different possible measures can be taken. One way to reduce peaks is by reducing load in times of high demand which for example can be done by shifting electrical heating to times of lower demand or activating additional generation units. Another method includes using a battery to shift the peak to times of lower demand by charging at demand valleys and later discharging at peaks and therefore smoothening them. Therefore, the energy for charging is bought in times of low prices and sold back in times of high energy prices.
- **Load leveling:** In difference to peak shaving the battery is used to level out the whole demand curve throughout the day. Therefore, a BESS with a higher usable energy capacity is needed as the storage demand is increased.
- **Power reserve:** The load demand is always predicted by the grid operator in advance and based on that, the operation of generation units is cleared. If the actual demand deviates from the forecast demand or if generation is not provided as forecasted, generation and demand do not match. To provide power reserve, batteries can be used to store energy from times of exceeding generation and discharge in times of exceeding load. The system owner is paid by the grid operator for the provision of this service. The amount of electricity that can be fed into the grid is based on a contract between the grid operator and the system owner.
- **Integration of volatile renewable energy sources:** As the integration of renewable energy sources grows constantly, the integration of the same to the grid becomes a challenge, as the generation is non-dispatchable and volatile due to weather conditions. On the one hand, this volatility can be tackled by installing batteries

and distributing the production based on the market prices. On the other hand, the implemented nominal power of renewables can be increased by batteries, as peak generation can be shifted to times of generation valleys therefore increasing the full load hours of the grid connection.

- **Frequency regulation:** The frequency is a global parameter for the stability of generation and demand and has to be kept inside narrow boundaries. If generation exceeds demand, the frequency increases, while it decreases if generation is lower than demand. To counteract this, batteries can be used to discharge by injecting active power into the grid if the frequency is below the nominal frequency and charge by extracting active power from the grid if it is beyond the nominal frequency.
- **Voltage regulation:** The voltage is a local parameter of a part of the electric grid. For injection to the grid, the voltage rises compared to surrounding nodes with no injection. If there are many nodes on the same line, that inject at the same time, the voltage level can exceed the boundary of the allowed voltage range. If contrarily too much power is extracted the voltage decreases. As a countermeasure the BESS can be used to work as a reactive power source to the grid locally to increase the voltage and contrary work as a reactive power drain to reduce the voltage.
- **Uninterruptible power supply:** In case of outages, batteries can be used to ensure an uninterruptible power supply for critical applications over a given time. These critical applications can for example be monitoring systems, emergency lighting and medical equipment.

In 2017, the highest share with 50% of total rated BESS power was dedicated to frequency regulation, followed by reserve capacity, electricity bill management and electricity time shift with around 8 - 10% [4]. In combination with PSHP, a BESS can be used to deliver frequency containment reserve (FCR), where the main benefit of the BESS is volatility reduction in PSHP and therefore extend the lifetime of wearing parts [5]. This is for example done with the Blue Battery, the biggest Austrian power plant-connected battery, with a net power of 8 MW and an energy capacity of 14.2 MWh. This BESS is operated by Verbund at the run-of-river power plant in Wallsee-Mitterkirchen, Austria [6].

2.2 Floating photovoltaic systems

FPV is an opportunity to increase PV installation capacities in addition to land-based systems. The first installed FPV system had a nominal power of 20 kW in Aichi Province in Japan and was built in 2007 for research use. From this point onwards, installed capacity began to grow exponentially, leading to a cumulative installed FPV capacity of

1 314 MW in 2018. Until then, the biggest players were China with 73%, followed by Japan with 16% of the total installed power. [2]

Currently, the biggest FPV system in Central Europe is located in Grafenwörth, Austria with a net power of 24.5 MW. It has an estimated energy yield of 26 700 MWh per year and an area of approximately 140 000 m² [7].

2.2.1 Structure of a floating photovoltaic system

The structure of an FPV system is different from a land-based system in various ways, as it is mounted on top of a water basin. The structure of a basic floating photovoltaic system is depicted in Fig. 2.1 where the different components are shown. In the following a summary of the key components is given based on [2].

- **Floating platforms:** The PV modules are installed on a floating platform, which can vary in its used technology. Pure-floats designs use specially designed buoyant bodies to support PV panels directly, while pontoons with metal frames are closer to land-based systems. The pontoons only provide buoyancy, while the metal frame provides stability. Another type of platform is created by simply covering the entire water surface with rubber mats to create a base for PV installations.
- **Anchoring and mooring systems:** An appropriate anchoring and mooring system is a critical part of an FPV plant. There are three basic ways to hold a floating platform in place. Bottom anchoring is used in the vast majority of existing FPV plants, where usually a large concrete block is submerged and works as an anchor for the system based on its sheer weight. Bank anchoring is particularly suitable for small, shallow ponds, where the FPV plant is close to shore and should be considered, if possible, as it is often the most cost-effective option. For some (typically shallow) water bodies, it may be possible to drill or ram piles into the basin floor. The floating platform is then moored to the piles.
- **Electrical configuration:** Like ground-mounted PV plants, FPVs use either central inverters or string inverters for their electrical layout. For large FPV systems, it is advantageous to install the inverters on the water and not on land to avoid excessive cabling losses.

2.2.2 Advantages and disadvantages

Depending on how they are integrated, they can have various advantages over land-based systems and can be positively influenced by the existing infrastructure of water basins or hydropower plants. On the downside, there are also disadvantages, such as

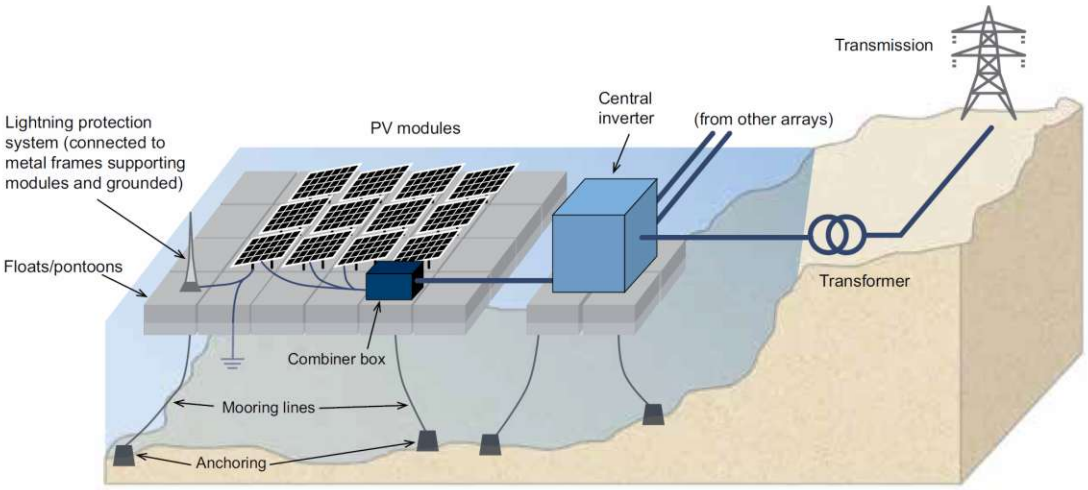

Figure 2.1: Structure of an FPV system [2]

higher initial investment costs. In the following paragraphs, some of the main advantages and disadvantages of FPV compared to land-based PV systems are discussed.

Advantages of FPV:

- **Increased energy yield:** As the FPV is installed near the water surface, the evaporative cooling effect tends to lower the module temperature, which leads to an increase in efficiency. Also, wind speed is usually higher close to the water surface, which further reduces the module's temperature. Additional reasons for higher energy yield are the facts that large water bodies are usually not shaded by nearby objects and they also tend to be less dusty. Therefore, the energy yield could be increased by up to 10% based on the global horizontal irradiation [2]. Another study, in which a comprehensive literature review was conducted, found that the operating temperature of FPV (at least for air-cooled modules) compared to land-based PV should not necessarily be considered lower [8]. Therefore, the evaporative cooling effect could also be small. In one study it is even stated, that the energy yield of FPV could be even less than for land-based systems, as the solar spectrum is decreased by the increased humidity due to evaporation [9]. Accordingly, research on this topic is still ongoing and the influence of evaporation on energy yield needs to be investigated further.
- **Reduced evaporation:** Due to the covering of the water body by the FPV, the effects of irradiation and wind on evaporation are reduced. Therefore, the loss of water can be decreased, which is crucial for countries where water is scarce

[2]. The effect of reduced evaporation by the FPV will become more and more important in the future due to rising temperatures and therefore increasing evaporation rates [10]. Worldwide, there are already many projects that make use of this advantage of reduced evaporation.

- **Reduced competition in land occupation:** Compared to land-based PV systems, FPV systems do not compete for land with agriculture, industrial and residential projects [2], especially in greatly industrialized areas [10]. Also, the permission process is often less complicated, as the water bodies often have a single owner [2].
- **Hybrid operation with pumped hydro storage power:** PV generation is a non-dispatchable way of providing electricity to the power grid. In combination with PSHP, it is then possible to store the energy generated for times when demand is higher. Therefore, the produced energy by the FPV can be used to pump water to the upper reservoir and discharge it for times with higher demand or when FPV generation is lower. Another advantage of hybridization is that the existing infrastructure can be used more efficiently. [2]

Disadvantages of FPV:

- **Initial investment costs** Due to the different mounting of FPV systems with both a buoyance and anchoring system the initial investment costs are currently higher than for ground-mounted systems. But with increasing competition and economies of scale, the future costs are assumed to decrease. [2]
- **Limited tilt angle** As high tilt angles of the FPV increase the effective surface exposed to wind, this would lead to higher forces on the anchoring and mooring system. Therefore, the tilt angle has to be lower than for land-based systems, which decreases the energy yield. [11]

2.2.3 Hybridization with hydro storage power

Additionally, to the already discussed advantage of FPV with pumped hydro storage power, this section will give a deeper insight into the already existing literature on hybrid operation. Also, estimations of the potential of FPV operation with hydro storage power are provided.

Based on the coverage of the reservoir surface, there is an estimated generation potential of 13.87 TWh/a for 1% coverage, 138.67 TWh/a for 10% coverage and 1386.7 TWh/a for 100% coverage for the whole EU. If the net power of the FPV is the same as the net power of the hydro power plant, the annual generation of the FPV systems would be 42.31 TWh. For context, the total generation from PV was 156 TWh in 2020, while the

total generation in the EU was 2780 TWh in 2019 [12]. On a global scale, the theoretical potential of FPV on PSHP reservoirs was estimated between 3 039 GW/4 251 TWh/a and 7 593 GW/10 616 TWh/a depending on the minimum and maximum shore distance of the FPV system [13].

In [11], the joint operation of FPV and the Alto Rabagão power plant (Montealegre, Portugal) on the day-ahead market is studied, for different days and scenarios. Different deviations from the forecast are taken into account on the one hand, and whether or not penalties for non-compliance are charged on the other hand. It has been found that joint operation makes sense, if penalties are charged. Without penalties, the pumping losses would be too high, so that joint operation would reduce revenues compared to the direct sale of FPV electricity on the day-ahead market.

A purely technical approach was chosen in [14], where the operation of a combined FPV and PSHP were compared to the single operation of an FPV system and a PSHP. The PSHP had total nominal power of 1 GW for pumping and turbining, while the FPV had a nominal power of 2 GW. The paper developed a dual-objective model for the cooperation of the hybrid FPV-PSHP plant, which simultaneously maximizes the generation benefits and minimizes the energy imbalance between generation and load. It was shown, that the combined operation can increase the utilization of the FPV from 31.82% in stand-alone FPV operation, to 86.62% in combined operation. The generation benefit was increased from 4701.37 MWh/d for stand-alone PSHP, to 9126.21 MWh/d for combined operation.

2.3 Own contribution

Based on the literature review, this thesis provides insights into the influence of the expansion sizes of a BESS and FPV system on the technical and economic KPIs of a PSHP. The use case for the hybrid system is an optimized operation for trading on the day-ahead market. Therefore, the FPV nominal power, the usable BESS energy capacity and the BESS storage duration are varied, and separate simulations are carried out in the form of a parameter study. Within this parameter study, a comparison is also made between the binary and ternary operation of the PSHP. The reduced evaporation due to the coverage of the PSHP reservoir by the FPV is investigated by implementing a regression model. This calculates the reduced evaporation based on the basic weather data and the degree of coverage of the water surface.

3 Methodology

3.1 Problem statement

In this thesis, a techno-economic assessment of a pumped storage power plant in a combined operation with an FPV and a BESS is conducted. Therefore, an existing storage power plant located in central Sweden, which will be refurbished and upgraded to a PSHP plant, is taken as a reference. The data for the technical components of the PSHP (turbines, generators, pumps, transformers) and general data for modeling the reservoirs and pipes are provided by Global Hydro. The data quality and availability of this site are therefore very high. As shown in Fig. 3.1, the PSHP consists of three different reservoirs, the lowest of which has a considerable storage capacity, while the middle reservoir is rather small. The power plant consists of two stages, that have their own grid connection with a transformer. In addition to the real PSHP, an FPV is simulated on top of the upper reservoir and therefore connected to the top stage of the PSHP. In addition, a BESS is simulated at the upper grid connection point, which can also store the output of the FPV. This hybrid power plant (HPP) is then operated for trading on the day-ahead market. For this purpose, an optimization model is created as a linearized abstraction of the technical model.

For the technical representation with detailed models of each technical component, the Austrian Institute of Technology's (AIT) TESCA (**T**ecno-**E**conomic **S**ystem and **C**omponent **A**nalysis) framework is used and extended by the components of the PSHP. This Python-based framework is used for steady-state simulation of different energy conversion and storage components. For this thesis, the ACDC converter and battery components are used while the components of the PSHP are newly modeled and introduced to the framework. A detailed description of those components can be found in the following section 3.2.

Based on this technical component model, an optimization model is set up for optimizing the operation for trading on the day-ahead market. This optimization model is a linearized representation of the component model, which is initialized using the current state of the components and time series input data (inflow of the upper reservoir, FPV profile, energy cost and revenue). For the optimization model, AIT's IESOpt (**I**ntegrated

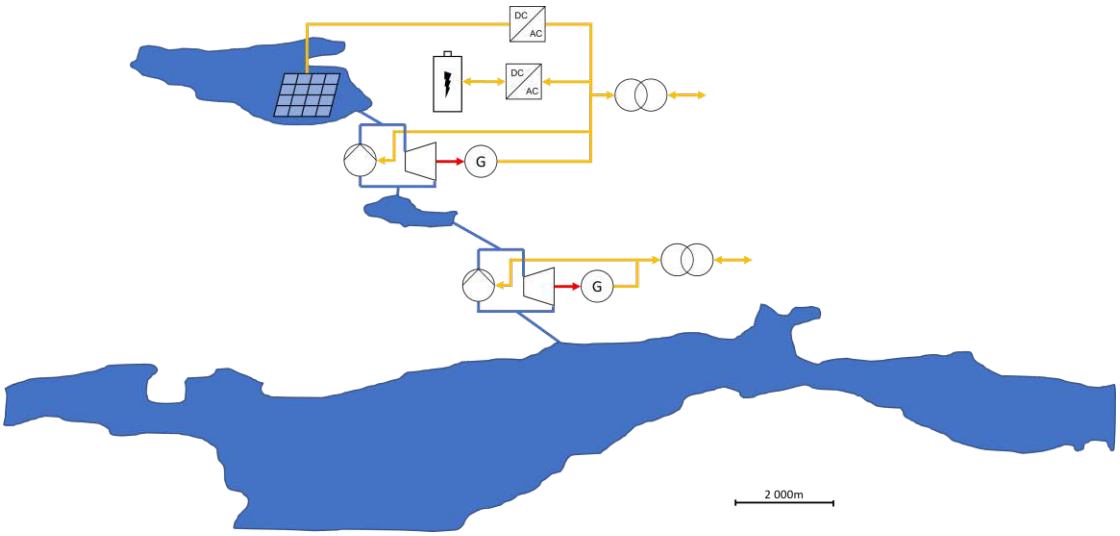

Figure 3.1: Schematic structure of the simulated hybrid power plant where the blue lines are representing the waterway, red lined the mechanic transmission and yellow lines the electric lines.

Energy **S**ystems **Opt**imizer) is used, which is a component-based optimization framework written in the programming language Julia. A closer description of this model is presented in Section 3.3.

As the optimization model is only used for finding the optimal operation of the HPP and not the sizing, a parameter study is conducted. Therefore, the nominal power of the FPV, the battery usable energy capacity and storage duration are varied in a specific range. Also, scenarios for binary and ternary operations are simulated. After the technical simulation, the economic viability is evaluated by calculating different KPIs and comparing the scenarios. The detailed descriptions of the KPIs are presented in Section 3.4.

With those technical and optimization models, the simulation of one specific scenario is then conducted as shown in Fig. 3.2. Therefore, the component model of the PSHP is initialized with the given input data provided by Global Hydro. Additionally needed weather profiles and market data are imported to the simulation. With this data and the component model, the optimization model is initialized and run. In one optimization run, the optimal set points for the whole system of the following three days are calculated. These set points are then handed over to the component model where this data series is then iterated and consecutively called. As the optimization model is only a linearized representation of the component model, there are deviations in the storage's state of charge inside the optimization and component models. In every iteration, it is checked whether the set point is actually possible based on the component's state

and is then clipped to possible values if needed. After every simulation step of the components, it is checked whether the storage's states of charge in the optimization and component model are deviating more than 1%. If so, a new optimization run is triggered before the optimization horizon of three days is reached. After simulating one whole year, the technical results are then passed on to the economic evaluation, which calculates the economic KPIs.

3.2 Component model

3.2.1 Reservoir

Geometry

For the reservoir, the decision is made, to model it with high flexibility in its measurements, instead of a simple approach with a state of charge that does not influence the area or the depth of the water body. This simple approach would lead to a reduced influence on evaporation and potential energy, leading to information loss. Therefore, the topography is cut into various slices of 2D plains, where the (x, y)-coordinates of each z-layer are the logical neighbors of the surrounding layers and therefore has a structure like shown below.

$$\begin{gathered} z_0 : (x_{0,0}, y_{0,0}), ..., (x_{i,0}, y_{i,0}) \\ ... \\ z_j : (x_{0,j}, y_{0,j}), ..., (x_{i,j}, y_{i,j}) \end{gathered}$$

Based on a given z-coordinate, the total area of one plain is calculated using the shoelace formula (also known as Gauss's area formula or surveyor's formula) by summing up the areas which are built by one line of the polygon and the x-axis, which is

$$A = \sum_{n=0}^{N-1} A_n = \sum_{n=0}^{N-1} \frac{(x_n - x_{n+1}) \cdot (y_n + y_{n+1})}{2} \tag{3.1}$$

where N is the number of corners of the polygon and $x_N = x_0$ and $y_N = y_0$. The underlying visual explanation is shown in Fig. 3.3, where the red area is considered negative and the blue one positive. Therefore, the sum of all such areas of a general polygon is its area.

For the calculation of a specific piece of volume between two neighboring layers, the approach of (3.1) can be extended as following. If the gradients of the (x,y)-coordinates

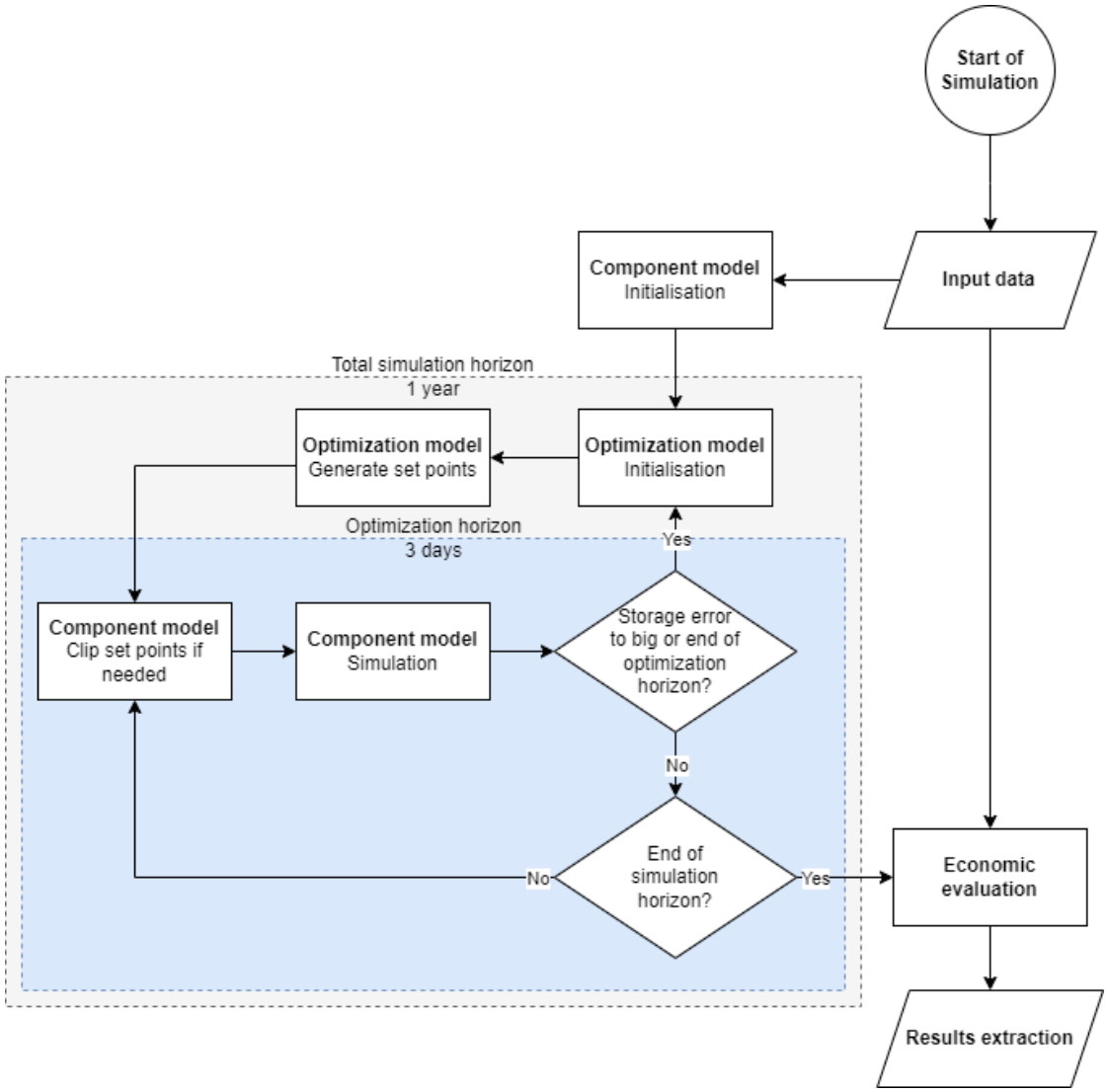

Figure 3.2: Flowchart of the simulation process

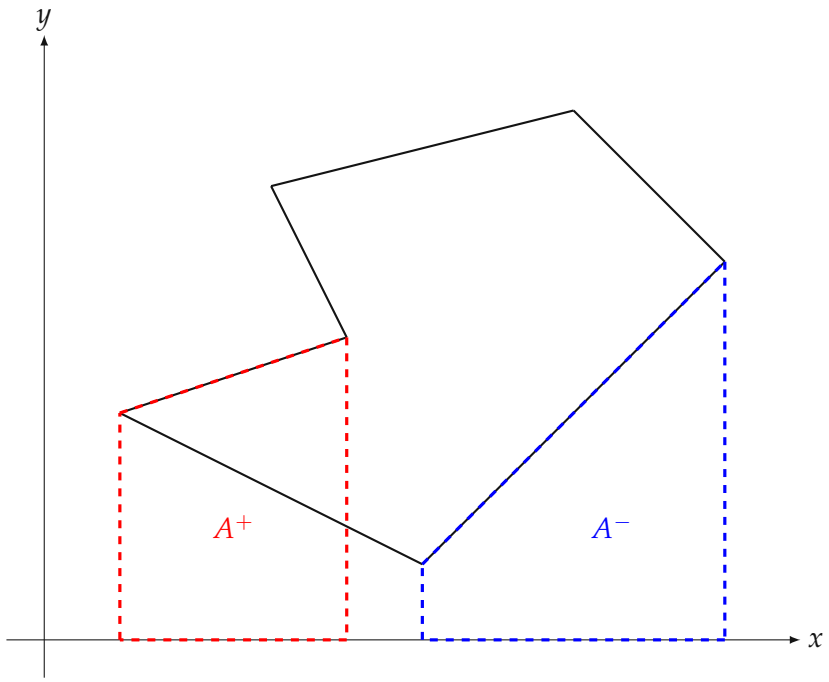

Figure 3.3: Visual explanation of how to calculate the area of a general polygon

of two logical neighboring points $P_{n,m} = (x_{n,m}, y_{n,m})$ and $P_{n,m+1} = (x_{n,m+1}, y_{n,m+1})$ for two neighboring planes at z-coordinates z_m and z_{m+1} are considered as

$$\frac{\Delta x_n}{\Delta z_n} = \frac{x_{n,m+1} - x_{n,m}}{z_{m+1} - z_m} \tag{3.2}$$

$$\frac{\Delta y_n}{\Delta z_n} = \frac{y_{n,m+1} - y_{n,m}}{z_{m+1} - z_m} \tag{3.3}$$

The area at a specific z-coordinate z^* in the range $[z_m, z_{m+1}]$ therefore is

$$A(z^*) = \sum_{n=0}^{N} A_n(z^*) \tag{3.4}$$

with

$$A_n(z^*) = \left[\left(x_{n,m} + \frac{\Delta x_n}{\Delta z_n} \cdot z^*\right) - \left(x_{n+1,m} - \frac{\Delta x_{n+1}}{\Delta z_{n+1}} \cdot z^*\right)\right] \cdot \left[\left(y_{n,m} + \frac{\Delta y_n}{\Delta z_n} \cdot z^*\right) + \left(y_{n+1,m} - \frac{\Delta y_{n+1}}{\Delta z_{n+1}} \cdot z^*\right)\right] \cdot \frac{1}{2} \tag{3.5}$$

By integration of (3.4) according to the z-coordinate, the volume between two z-coordinates is calculated as

$$V = \int_{z_0}^{z_1} A(z^*)dz^* = \sum_{n=0}^{N} \left(E \cdot \Delta z + F \cdot \Delta z^2 + G \cdot \Delta z^3\right) \tag{3.6}$$

where $\Delta z = z_1 - z_0$ is the difference between those two z-coordinates, which have to lie within two neighboring layers. For simplicity and better visualization, the constants E, F and G are introduced, which are

$$E = \frac{1}{2}\left(x_{n,0} - x_{n+1,0}\right) \cdot \left(y_{n,0} + y_{n+1,0}\right) \tag{3.7}$$

$$F = \frac{1}{4}\left[\left(x_{n,0} - x_{n+1,0}\right) \cdot \left(\Delta y_{n,0} + \Delta y_{n+1,0}\right) + \left(\Delta x_{n,0} - \Delta x_{n+1,0}\right) \cdot \left(y_{n,0} + y_{n+1,0}\right)\right] \tag{3.8}$$

$$G = \frac{1}{6}\left(\Delta x_{n,0} - \Delta x_{n+1,0}\right) \cdot \left(\Delta y_{n,0} + \Delta y_{n+1,0}\right) \tag{3.9}$$

Evaporation

To estimate the amount and further the influence of evaporation on the water bodies, an estimation based on [10] is implemented. In this paper, the evaporation is calculated based on different evaporation models from the literature and compared to measured data. As these models are often very complex and require substantial input data, regression models were created on this basis. The precision of these linear regression models was then further tested on the measured data of a water basin (Biviere Lake in Lentini Catania, Italy). Based on the input data needed, the regression model for an estimated evaporation

Table 3.1: Relative reduced evaporation for three different FPV cover types [10]

Percentage of covering [%]	0	10	30	50	70	100
ΔE_{Full} [%]	0.0	19.0	51.0	75.0	90.2	100.0
$\Delta E_{Suspended}$ [%]	0.0	5.7	17.0	28.4	39.7	56.7
$\Delta E_{Flexible}$ [%]	0.0	15.2	42.1	64.4	82.0	100.0

$$\begin{aligned} E = &-0.307 - 0.0486 \cdot R_S + 0.177 \cdot T + 0.0119 \cdot RH + 1.00781 \cdot u_{10} \\ &+ 0.00163 \cdot R_S \cdot T + 0.00098 \cdot R_S \cdot RH - 0.00601 \cdot R_S \cdot u_{10} \\ &- 0.00244 \cdot T \cdot RH + 0.0153 \cdot T \cdot u_{10} - 0.0115 \cdot RH \cdot u_{10} \\ &+ 0.0045 \cdot R_S^2 + 0.00248 \cdot T^2 - 0.0109 \cdot u_{10}^2 \end{aligned} \tag{3.10}$$

is chosen, where R_S is the horizontal solar radiation in $\left[\frac{MJ}{m^2 d}\right]$, T the mean daily temperature in $[°C]$, RH the mean daily relative humidity in $[\%]$ and T mean daily wind speed 10m above the ground in $\left[\frac{m}{s}\right]$. [10]

Evaporation reduction

Based on the energy household of a water basin, the reduction in evaporation for different cover types is modeled in [10]. Even though the paper focuses on the reduced evaporation based on FPV, the reduced evaporation is included in the model of the reservoir. This decision is based on the influence of the cover on the reservoir and it is considered, that the reduced evaporation is not limited to covering by FPV, but rather by a specific type of cover. As an FPV can be installed in various ways, three different cover types are looked at, which are full (Fig. 3.4 (A)), suspended (Fig. 3.4 (B) and (C)) and flexible covering (Fig. 3.4 (D)). For those three cover types, the reduced evaporation is calculated by interpolating over the reduced evaporation, based on the relative cover area, which is shown in Tab. 3.1. [10]

Programmatic implementation

According to the technical description a Python class is implemented for the reservoir. For initializing there are various measures needed to set up the object. With the coordinates of the boundaries of the reservoir, a translation table based on (3.4) and (3.6) for the area and volume are calculated for a specific number of filling levels. Using this, also the corresponding state of charge (SOC) is calculated. This is done

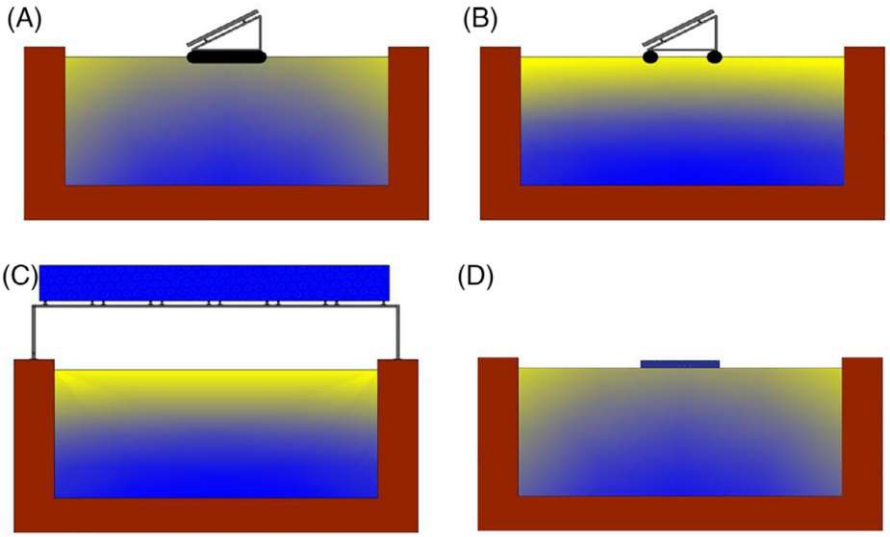

Figure 3.4: Typologies of FPVs mounting structure: (A) the floats cover the entire surface below the module; (B) The modules are anchored to a buoyancy system; (C) The PV is implemented as a canal top solar systems; (D) flexible floats [10]

in the initialization, to reduce runtime in the following simulation. The object is also initialized with an initial SOC and the maximum depth of discharge (DOD), which should not be undercut in the simulation. Additionally, it can optionally be specified if evaporation should be further considered and if a cover is used.

3.2.2 Waterway

Loss head and efficiency

The waterway of the PSHP consists of various elements, which contribute to the total losses, mostly due to friction. Examples are the rake at the water inlet for stopping large objects from getting into the downpipe, elbows, transitions, constrictions and many more. As stated in [15], the losses of the entire waterway can be calculated solely by the losses from friction in the downpipe as the other losses are negligible.

The efficiency of the downpipe is calculated with the approach of Darcy-Weisbach over the loss head

$$h_{loss} = \lambda \cdot \frac{L}{D} \cdot \frac{v^2}{2g} \tag{3.11}$$

where λ is the loss coefficient, L the length of the pipe, D the diameter of the pipe, v the diligence speed and g the gravity. When assuming that the pipe is shaped circularly, the Darcy-Weisbach equation is transformed to

$$h_{loss} = \lambda \cdot \frac{L}{D^5} \cdot \frac{8Q^2}{\pi^2 g} \tag{3.12}$$

where Q is the flow through the downpipe. The loss coefficient λ is calculated using the Prandtl-Colebrook equation

$$\frac{1}{\sqrt{\lambda}} = -2log_{10}\left[\frac{2.51}{Re\sqrt{\lambda}} + \frac{k/D}{3.71}\right] \tag{3.13}$$

where k is the equivalent sand roughness and Re the Reynolds number. As $Re > 10^5$ the first term can be neglected and therefore, the loss coefficient is explicitly calculated with

$$\lambda = \frac{1}{4 \cdot log_{10}^2\left(\frac{k/D}{3.71}\right)} \tag{3.14}$$

and therefore, the loss head is

$$h_{loss} = \frac{2}{\pi^2 g} \cdot \frac{L \cdot Q^2}{log_{10}^2\left(\frac{k/D}{3.71}\right) \cdot D^5}. \tag{3.15}$$

Programmatic implementation

A Python class is created to represent the behavior of the downpipe and takes the equivalent sand roughness, length and diameter as parameters for initialization. The class also has methods for calculating the loss head, which is used in the pump and turbine classes.

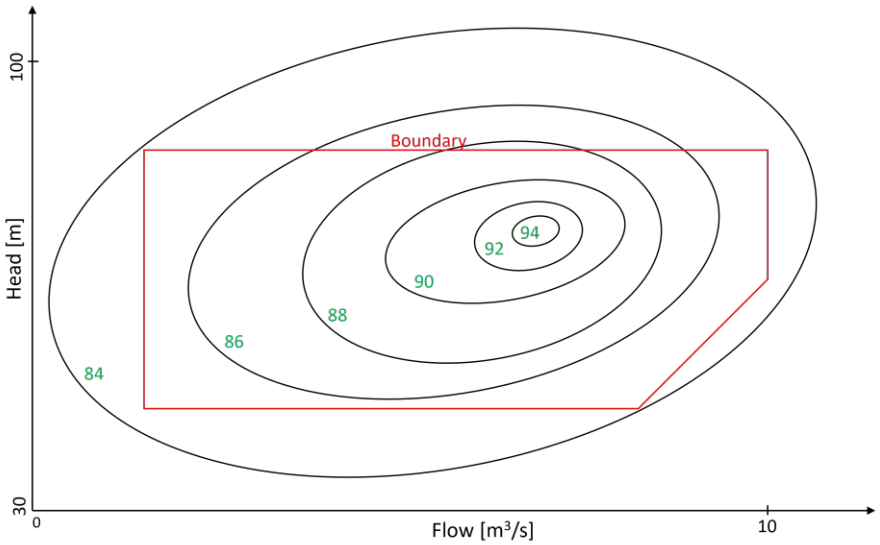

Figure 3.5: Exemplary hillchart of a turbine with the contour lines of the efficiency (green value in %) for a range of the effective head and the water flow, while the red line is the operational boundary for possible operation parameters

3.2.3 Turbine

Technical description

The turbine's technical behavior is modeled, using hillcharts which show the relation between the effective head, the water flow and the efficiency. Such an exemplary hillchart is shown in Fig. 3.5, which does not depict the real data used for this modeling, as this kind of data is restricted. Nevertheless, the graphic shows the basic structure of a hillchart and approximately reflects the data used. As shown, different efficiencies arise for different constellations of effective head and flow rate. The lines of the same efficiency then form the so-called hillchart, as it looks like the contour lines of a hill in a topographic map. As it is stated in 3.2.2, the effective head is not equal to the actual geodetic head, as friction inside the downpipe leads to a loss head.

The data of the received hillcharts for both the upper and lower PSHP stage are extracted using the WebPlotDigitizer [16]. As shown in the exemplary hillchart in Fig. 3.5, the area without information about the efficiency between those efficiency lines is relatively wide, compared to the part with information. In the following, it is necessary to find interpolated values for the mechanical output power with effective head and flow as input on the one hand and for flow with effective head and mechanic output power as input on the other hand. Therefore, it is necessary to expand the

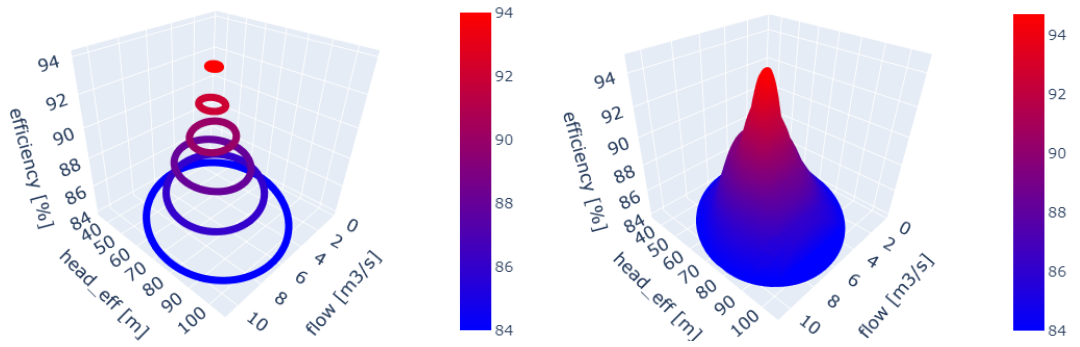

(a) Original hillchart data

(b) Prepared hillchart data

Figure 3.6: Comparison of the raw data of the hillchart, to the hillchart with higher granularity after cubic spline interpolation

data, to get rid of interpolation errors which would result in a mismatch. This is done by setting up a 2D mesh grid of effective head and flow and then interpolating the efficiency for this dataset. For this purpose, a cubic spline interpolation is chosen. The comparison of the raw and the processed data is depicted in Fig. 3.6, where the hillchart is transformed into a smooth surface. This allows a reduction of the interpolation error, due to interpolating back and forth between flow and mechanic power as input for the interpolation, additionally to the effective head.

Programmatic implementation

The turbine class is initialized with the so-prepared hillchart data, the boundary data and additionally a downpipe object. As the hillchart data consists of data points of effective head, flow and efficiency, the downpipe is used to calculate the loss height for each data point based on the flow (see 3.2.2) and is then added to the effective head

$$h_{act} = h_{eff} + h_{loss} \tag{3.16}$$

to calculate the actual head. Additionally, the mechanic output power is calculated as

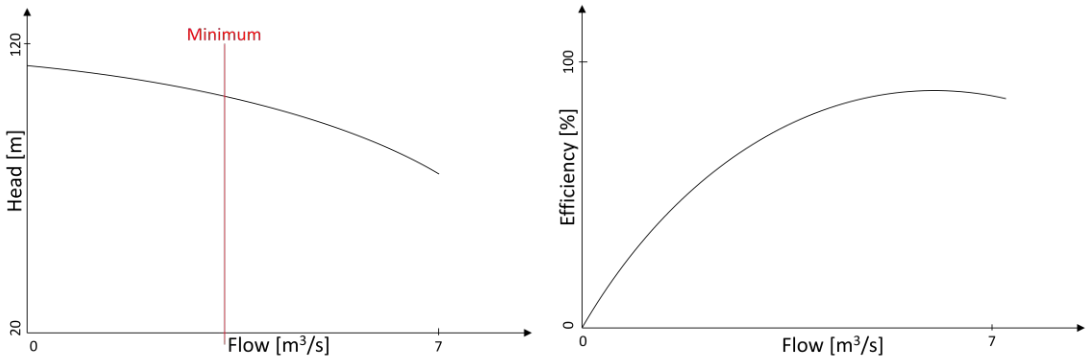

(a) Effective head over flow

(b) Efficiency over flow

Figure 3.7: Exemplary data of a pump data sheet, showing the relation between effective head, efficiency and flow

$$P_{mech,out} = \rho \cdot Q \cdot g \cdot h_{eff} \cdot \eta \tag{3.17}$$

where $\rho = 997kg/m^3$ is the density of water, Q is the flow, $g = 9.81m/s^2$ is the gravitation, h_{eff} the effective head and η the efficiency. With this method, an extended hillchart is created and stored in the turbine object as an attribute. Also, the boundary data is transformed in the same manner as with the hillchart data and is then also stored as an attribute in the turbine object.

3.2.4 Pump

Technical description

The model of the pump is based on the data provided by Global Hydro. The pumps used are driven by a synchronous machine without inverters for variable rotation speed. Exemplary representations of the data sheets are depicted in Fig. 3.7, where the connection between effective head, flow and efficiency is shown. There is only one specific flow for a given effective head, as the pump is driven by a synchronous machine without a frequency converter. The operating point for a specific geodetic head results at the intersection of the pipes characteristic curve and the pump characteristic curve [15]. It is therefore not possible to set the electrical output of the pump to any value.

Programmatic implementation

Based on the technical description above, a Python class is created to model this behavior. For the initialization of the pump object a dataset with the data extracted from the data sheets with the WebPlotDigitizer [16] is used and based on that information the actual head is calculated with

$$h_{act} = h_{eff} - h_{loss} \tag{3.18}$$

where h_{loss} is the loss head calculated with the downpipe object. Also, the dataset is extended by the resulting electric power input with

$$P_{el} = \frac{\rho \cdot Q \cdot g \cdot h_{eff}}{\eta} \tag{3.19}$$

for easier interpolation between those values.

3.2.5 Generator

Technical description

The behavior of the generator is a simple relation of the electric output power and the efficiency, which is exemplary shown in Fig. 3.8 and is based on data of a synchronous machine.

Programmatic implementation

Based on the technical description a Python class is set up. The object is initialized with the given data which, is extended by the mechanic input power

$$P_{in} = \frac{P_{out}}{\eta} \tag{3.20}$$

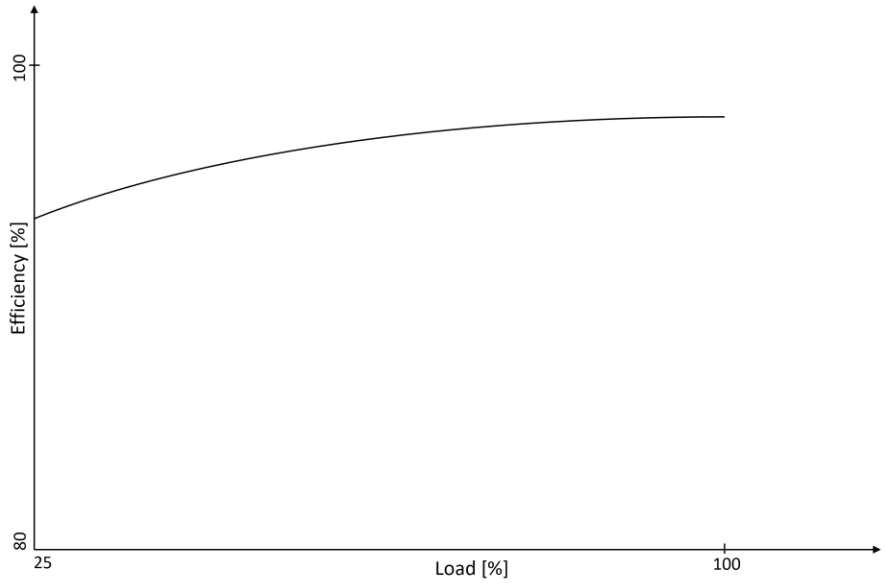

Figure 3.8: Exemplary data of a generator data sheet showing the relation between efficiency and load

3.2.6 Battery

AIT's TESCA-framework already contains a mature component model of the battery, which includes aging models and underlying battery losses. The aging model is described by both calendar and thermal aging, while the losses include active and passive losses. Active losses happen for charging and discharging the battery, while passive losses also occur in the standby mode of the battery, and therefore independent of the battery power. Based on the aging of the battery, the state of health and therefore the usable energy capacity of the battery is reduced.

3.2.7 ACDC-Converter

Like the battery, the ACDC-converter is also an already implemented class inside AIT's TESCA-framework and therefore is not specifically modeled for this thesis. The converter class works based on an underlying efficiency curve, which depends on the power set point of the converter. The object is initialized solely by the nominal power.

3.2.8 Transformer

Technical description

The transformer is modeled with a constant efficiency which does not vary for different power set points.

Programmatic implementation

As the technical input data to the Python class of the transformer is rather sparse, the implementation is also simple. The object's initialization is done by a constant efficiency and a nominal power which sets the maximum allowed power transfer.

3.3 Optimization model

Based on the initialized technical model of the whole system, a linearized optimization model is built using IESOpt. IESOpt is an energy system optimization framework of the AIT based on the programming language Julia. With this optimization framework, different types of components can be modeled. For this thesis, the component types unit, node and profile are used and initialized accordingly.

A **unit** is a component that has a set of inputs, a set of outputs and a conversion function, which defines the correlation between them and therefore defines the transmission ratio. In simple cases, like for the ACDC converter, the conversion is the same as the efficiency, while for the turbine it defines the relation between flow and output power. The units are also modeled with a minimum and maximum operation point, in between of which the operation is allowed. The transmission ratio is defined on both values and linearized in between. Therefore, the optimization problem is a mixed integer linear problem or MILP.

A **node** is a component that is used to balance the values between different units and/or profiles and can optionally be initialized with a state. This state is needed, if the inputs and outputs of a node do not have to be the same at each timestep. Therefore, the difference of both is stored in the node. This behavior is used to model the three reservoirs as well as the battery. Between two units, a node is mandatory to balance the flow between them, like in Kirchhoff's current law.

A **profile** can either be a profile of values or a profile of costs. The profile of values is used to model the FPV profile, the sink needed for destroying energy as FPV power needs to be curtailed and also for the inflow of the upper reservoir. The profile of costs

is used to model the costs and revenues for buying and selling from the day-ahead market.

The specific model for this study is then built based on those three components and is displayed in the following Figures 3.9 and 3.10. These figures are split up for better visualization of the model and are connected at the transformer units. Therefore, for example, the unit „Trafo from grid upper", has one path exiting to „Node upper" in Fig. 3.9 and one entering from „Grid buy" in Fig. 3.10. This also applies to the other transformer units.

As the unit component is only capable of one-directional conversion, the two transformers and the battery converter have to be split up into two units for each direction of power flow. Both directions are initialized with the same values and therefore are ultimately the same.

The FPV is represented as a profile which is initialized with the FPV profile. This profile is connected to another profile „FPV curtail", which is initialized as a sink. This enables the optimization model to curtail the FPV profile when the BESS is full and not all of the electricity generated can be fed into the grid or consumed by the pump. The inflow of the upper reservoir is represented as a profile, initialized as a source with specific values. The profiles „Grid buy" and „Grid sell" are initialized with the energy costs and revenues as described in Subsection 3.5.3.

3.4 Economic evaluation

For analyzing the economic viability, two different economic KPIs are calculated over the whole lifetime of the HPP by expanding the results of one year of operation for every simulation. The economic parameters used for the components are shown in Tab. 3.5. The KPIs looked at in this simulation study are the levelized costs of electricity (LCOE) and the net present value (NPV).

The LCOE are the average net present costs of electricity generation, which are calculated with

$$LCOE = \frac{\sum_{t=0}^{T} \frac{CAPEX_t + OPEX_t + C_{el,t}}{(1+WACC)^t}}{\sum_{t=1}^{T} \frac{E_t}{(1+WACC)^t}} \tag{3.21}$$

where $CAPEX_t$ are the capital expenditures, $OPEX_t$ the operational expenditures, $C_{el,t}$ the costs for energy extracted from the grid, $WACC$ the weighted average costs of

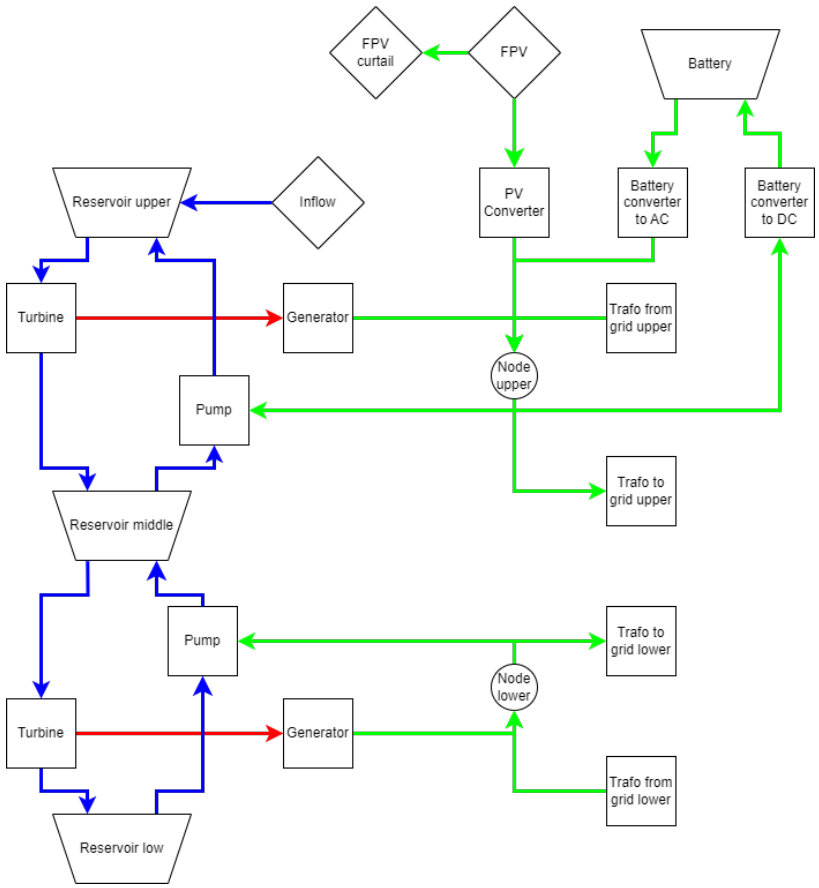

Figure 3.9: Representation of the optimization model, without the representation of the grid, where the trapezoids are nodes with states (storage), the squares are units and the diamonds are profiles. The carriers are blue for water flow, red for mechanic power and green for electric power. For better visualization, the mandatory nodes between turbines and generators are not displayed.

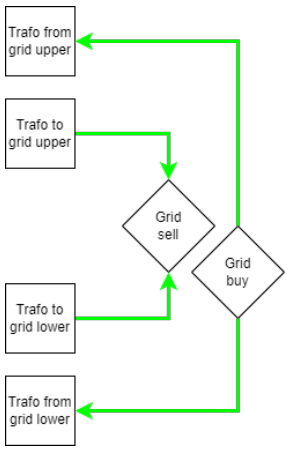

Figure 3.10: Addon of the grid to Fig. 3.9

capital and T the total period under review ()which is set to the lifetime of the PSHP). The $OPEX_t$ and $C_{el,t}$ are zero for $t = 0$, while the $CAPEX_0$ are the initial investment, which has to be raised before the first year of operation. In general, if the LCOE are higher, the average costs for an energy unit are higher.

The NPV shows whether a given system is profitable or not. It is calculated with

$$NPV = \sum_{t=0}^{T} \frac{R_{el,t} - CAPEX_t - OPEX_t - C_{el,t}}{(1 + WACC)^t} \tag{3.22}$$

where $R_{el,t}$ are the revenues by feeding energy into the grid and are zero for $t = 0$ like the $OPEX_t$ and $C_{el,t}$. A system is economically viable if the NPV is positive, as the discounted revenues exceed the expenditures.

3.5 Input data

3.5.1 Pumped storage power plant

The technical model of the whole HPP is set up as shown in Fig. 3.1. The data for the component initialization of the PSHP plant is provided by Global Hydro and is not changed throughout the parameter study. Therefore, the base case is defined as the operation of the PSHP, without integration of BESS and FPV. The usable energy capacity of the battery, the nominal power of the BESS converter and the nominal power of the FPV are varied in a defined set of parameters, to get an insight on the influence of these

Table 3.2: Input parameters for the downpipe objects

Stage	k mm	L m	D m
Upper	0.05	2300	2
Lower	0.05	2200	2

Table 3.3: Parameters used for initialization of the reservoirs

Reservoir	V $Mio.m^3$	A km^2
Top	61	5.8
Middle	0.163	0.3
Base	147	47.3

parameters on the technical and economic KPIs. This is done via a parameter study. Inside this parameter study the operation in binary and ternary mode of the pumps with the turbines is also considered. Therefore, the model is simulated various times and the results of each simulation are then stored for the economic evaluation, which is calculated based on the technical results.

The turbine, generator, pump, and transformer for both stages are initialized by the given data of Global Hydro. For the reservoirs, the area is roughly estimated by using basic functions of Google Earth, while the volume and the net head of the two stages are also provided by Global Hydro. The net head between the upper and middle reservoir is 99 m and between the middle and base reservoir, it is 75 m. The 3D data of the reservoirs needed for initializing the objects is estimated based on the given volume and surface area, which are shown in Tab. 3.3. The two downpipes are initialized with the data provided by Global Hydro and data extracted from Google Maps, while the equivalent sand roughness is assumed for a steel pipe [15] (see tab.3.2). The nominal active power of the upper and lower generator are set to 9090 kW and 6570 kW. These values are also used for the nominal active power of the transformers. The minimum and maximum flow of the turbines and pumps are shown in Tab. 3.4.

The weather data needed for the calculation of the evaporation from the reservoirs and generation of the FPV profile, EnergyPlus weather data from Meteonorm is used. Therefore, a data point in the region of the PSHP plant is selected and the data is extracted for the year 2022. As the data does not meet the conditions of its purpose, the units are adapted according to the units of (3.10), respectively the input format of pvlib (see 3.5.2).

As the FPV is simulated on the top reservoir, the cover area of the same is set to 10 m^2

Table 3.4: Rough boundary data of the pumps and turbines

Reservoir	Q_{min} $\frac{m^3}{s}$	Q_{max} $\frac{m^3}{s}$	h_{min} m	h_{max} m
Turbine upper	4.1	11.5	64	147
Turbine lower	3.9	10.45	45	98
Pump upper	4.7	8.1	89	120
Pump lower	4.4	7.6	70	93

per kW of nominal FPV power [17] and the FPV floating device is assumed to be of suspended type. Also, an inflow is assumed for the upper reservoir, wherefore data of the owner of the PSHP plant is used. The average inflow in the year 2022 is roughly 3 m^3/s.

Due to the complexity of the input data, optimization over a full year with hourly time steps is not possible, as it does not converge after hours of simulation. Therefore, the optimization horizon is reduced to the upcoming three days with hourly resolution. This practice leads to the problem, that an operational strategy has to be implemented for PSHP. Otherwise, it would turbine as much as possible to maximize profit when no final state of charge is required. It is assumed, that the reservoirs follow a seasonality over the year. Therefore, the energy content of the water reservoirs and hydro storage plants of the associated balancing group is drawn from the ENTSO-E Transparency Platform [18]. This profile is depicted in Fig. 3.11 and is implemented scaled to the nominal volume of the upper reservoir. In the optimization model, the reservoir filling of the upper reservoir at the end of the optimization horizon is then set to the value at the given time of the year. The final storage level of the middle and lower reservoir in the optimization model is 50% for the whole simulated year.

3.5.2 Floating photovoltaic

In difference to the other technical components, the FPV is not introduced as a Python model in the TESCA-framework but is set up with the Python package pvlib [19]. This package generates the FPV generation profile based on simple weather data, albedo and the nominal power. The minimal requirement for the weather data is the direct normal, direct horizontal and global horizontal irradiance and the optional data are air temperature, cell temperature, module temperature, wind speed and albedo. In this thesis, all of the above are used as input, except the cell and module temperature, as meteonorm is used as a source for weather data and therefore does not offer those plant-specific data. Further needed input parameters are the tilt, azimuth, converter losses and the temperature coefficient. As the converter is separately modeled using

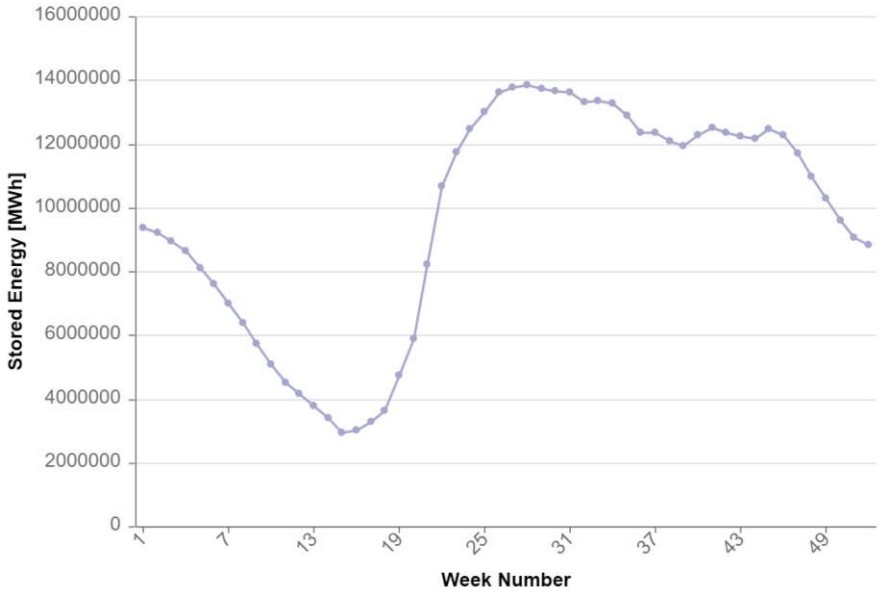

Figure 3.11: Aggregate filling rate of water reservoirs and hydro storage plants of the associated balancing group for the year 2022 [18]

the TESCA-framework, the converter losses are set to zero. The temperature coefficient of the PV is set to -0.4%/K, as a crystalline silicon PV module is assumed for the FPV system.

Even though different studies state that evaporation and the direct proximity to the water increase the efficiency of a PV system, due to reduced cell temperature [17], [20], others state that this effect is rather small or negligible [8]. Some even propagate a lower energy yield compared to land-based PV systems due to the decreased solar spectrum [9]. Given this inconsistency in the literature, it is simplistically assumed that the FPV profile is the same as for land-based PV.

The orientation of the FPV is restricted to a maximum tilt of 15°, as a steeper tilt would lead to a need to enforce the anchoring of the FPV as the impact of wind increases for higher tilt angles [17]. The ideal tilt and azimuth are then found by simulating the FPV with varying values of both parameters and summing up the annual generation. This leads to an orientation with a 15° tilt and an azimuth of 174°, for which the cumulative generation is highest. The resulting profile for one year is displayed in Fig. 3.12, where the power is shown as a percentage of the nominal power. There is a high degree of seasonality, which is caused by the location of the PSHP in central Sweden. The maximum power of the FPV is roughly 80% of its nominal power.

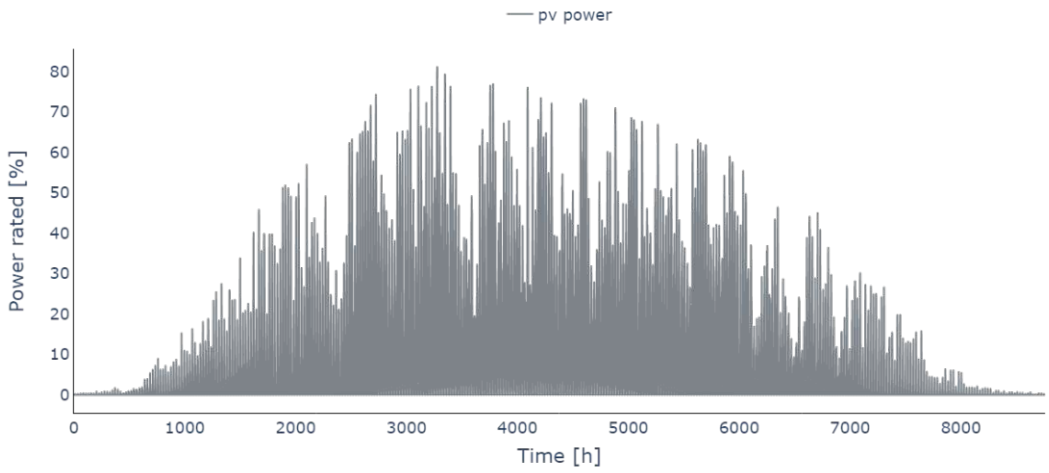

Figure 3.12: Rated FPV profile of one year

3.5.3 Day-ahead market and grid charges

The day-ahead market data of the balance group is drawn from the ENTSO-E Transparency Platform [21] for the year 2022. For the representation of the grid charges, the costs of the transmission system operator Svenska Kraftnät are taken as reference [22], which are separated into power and energy-related costs. The power related costs are 98 SEK/(kW·a) for the consumption and 65 SEK/(kW·a) for feed-in. As they represent the investment costs of the grid, they are multiplied by the maximum possible grid connection power, which is set to the nominal active power of the transformers. The energy-related costs are calculated based on the day-ahead price with

$$C_{t,E} = (C_{t,DA} + r) \cdot F \tag{3.23}$$

where $C_{t,DA}$ is the day-ahead price for a given timestep, r is the risk mark-up of Svenska Kraftnät with 10 SEK/MWh and F is the loss coefficient for the given connection point, which in this case is 5.2%.

3.5.4 Component costs and lifetime expectations

The assumptions for costs and lifetime of all components are shown in Tab. 3.5. While the costs and lifetime expectations of the whole PSHP including the transformers are assumptions made by Global Hydro, the other data is derived from literature. The

Table 3.5: Asset costs and lifetime expectations

Component	CAPEX -	OPEX *% of CAPEX p.a.*	Lifetime *years*	Source
PSHP + Transformers	21.5 Mio. EUR	4	30	Global Hydro
FPV system	1 260 EUR/kWp	1.2	30	[23]
FPV inverter	7.8 EUR/kW_{DC} [a]	0 [b]	10	[23]
BESS (duration 4 h)	405.9 EUR/kWh	2.5	15	[24]
BESS (duration 2 h)	488.7 EUR/kWh	2.5	15	[24]

[a] Follow-on investment for inverter replacement, as it is assumed with a lifetime of 10 years and the first investment is included in the CAPEX of the FPV system; [b] Included in the OPEX of the FPV system

costs of the FPV system include the costs of the modules, anchoring, floats, cabling and inverter, with a total lifetime of 30 years. Every 10 years, the inverter has to be exchanged, which is represented by the FPV inverter costs in the subsequent line [23]. The costs of the BESS cover all costs including the BESS inverter [24].

4 Results and discussion

Following the methodology of the previous chapter 3, the results are presented and discussed based on the research questions in section 1.2. In the first two sections of this chapter, the overall results are discussed with regard to the technical (section 4.1) and economic evaluation (section 4.2). Then the influence of FPV on the reduction of evaporation is discussed in section 4.3. While only the binary operation of the pumps is considered in these three sections, a comparison to ternary operation is made in section 4.4.

4.1 Technical evaluation

4.1.1 Base case

Due to the operation strategy of the PSHP, the utilization of the turbines and the pumps is rather seasonal, as displayed in Fig. 4.1 for the base case without FPV and BESS integration. Positive values of the power are referring to feed-in to the grid and negative to extraction from the grid. During summer, both stages follow the given state of charge of the upper reservoir, by pumping most of the time. In spring and late fall to early winter the PSHP is mostly in turbining operation. Throughout the rest of the year, the PSHP can be used for arbitrage and therefore, gain higher rates of revenue, as it is not as limited by the operation strategy. In general, the overall behavior of both stages is rather similar, with the difference, that at the lower stage the power is lower than at the upper. This can be explained by the bigger head of the upper stage compared to the lower one. In some cases, the upper and lower stage have a different grid transfer power, as the flow of both stages is not the same and the volume in the middle reservoir is not always perfectly at 50% after the three days of the optimization horizon. Therefore, the filling level must be adjusted by having a highly different flow in the two stages. While the power of the lower stage is more or less the same for both pumping and turbining, it is observed, that the upper stage has a varying power for both cases. This is due to the bigger variation in the geodetic head of the upper stage, following the operation strategy and the comparably high volume of the lowest reservoir, which keeps the filling level rather constant. The head of the upper stage is in the range of 95 to 105 m

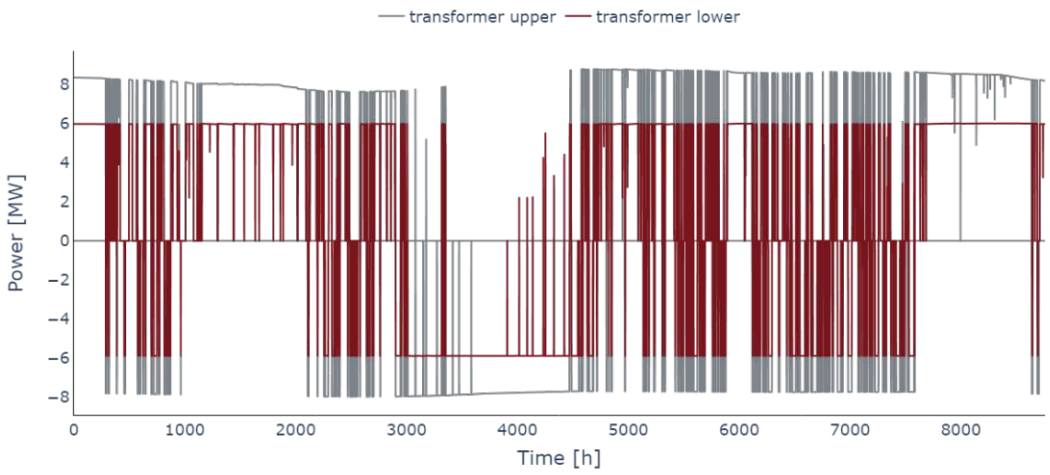

Figure 4.1: Power transfer between the PSHP plant and the grid at the upper and lower grid connection in the base case without FPV and BESS integration

throughout the year, which leads to a total head difference of 10%. This also applies to the potential energy, as it is linearly dependent on the head. The head of the lower stage is rather constant around 75 m.

The resulting SOC of the actual reservoir content in relation to the usable storage volume of the top and middle reservoir during the year are shown in Fig. 4.2. In this figure, also the comparison between the SOC of the optimization model and the thereof resulting SOC of the technical simulation is shown. The SOC of the top reservoir is more or less following the operation strategy. The ripple is derived from the arbitrage during the three days of the optimization horizon, as the SOC only must meet its final state and can operate more or less freely during this time. In comparison to the top reservoir, the middle reservoir has a higher fluctuation in the SOC, as its volume is far smaller. For comparing both the SOC within the optimization model and the technical model it is apparent that the deviation is higher for the middle reservoir. This results from the smaller reservoir capacity and therefore the relative filling is affected more by deviations from the expected flow. As shown in the flowchart of the simulation process in Fig. 3.2, the middle reservoir usually leads to a restart of the optimization model before the end of the three days of optimization horizon. These newly triggered optimization runs can be recognized by the fact that the SOC of the technical model deviates increasingly from that of the optimization model and then the SOC of the optimization model abruptly returns to that of the technical model (like around the 3800^{th} hour of the year). This abrupt return is the result of the new initialization of the optimization model with the actual SOC of the technical model.

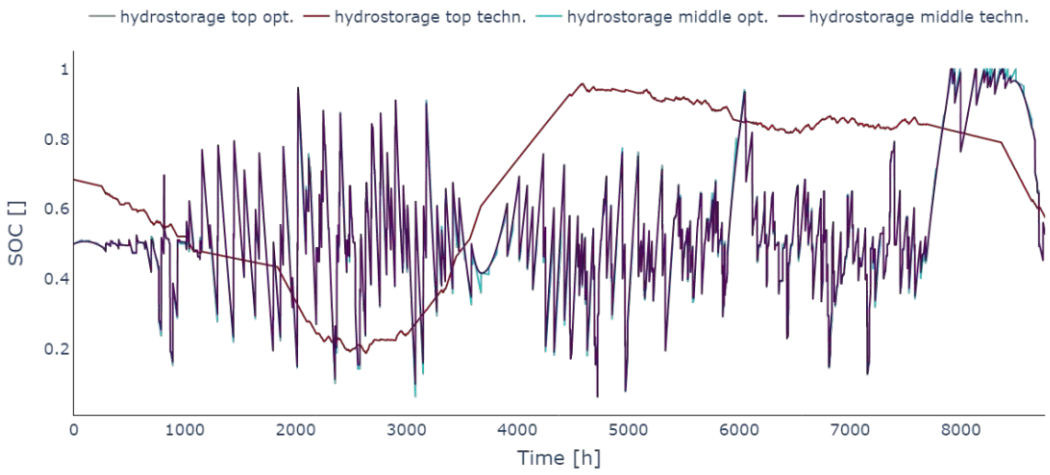

Figure 4.2: State of charge of the top and middle reservoir. Also both the state of charge of the technical model and inside the optimization model are shown.

4.1.2 Integration of FPV and BESS

In Fig. 4.5 the grid connection power of the upper stage is shown for different nominal power levels of the FPV. As the FPV is connected to the transformer of the upper stage, only the grid power of this stage is examined. The valley in summer is filled increasingly with rising nominal FPV power, as the power needed for pumping is delivered directly by the FPV. The additional power in the spring added on top of the generated power from the turbine is rather constant for increasing nominal FPV power, as the transformer limits the feed-in to the grid. All in all, the total energy fed into the grid increases and the energy extracted is decreased. Not shown in this figure is that the FPV is not fully utilized as the transformer limits the power transfer. As depicted in Fig. 4.4, the possible FPV power is already curtailed in spring and fall for a nominal FPV power of 9.1 MW. For increasing FPV integration the annually curtailed FPV energy is increasing, as a higher amount of power is curtailed in times of increased turbine use and during increased pump use.

As up to this point solely FPV integration is discussed, in Fig. 4.5 the combined integration of both FPV and BESS are shown by depicting the load duration curve for both without a BESS and with a BESS with a usable energy capacity of 10 MWh and a storage duration of 2 h. The absolute values of the FPV power without BESS (Fig. 4.5a) show a plateau at approximately 9 MW as this is the net power of the associated transformer and therefore FPV output is curtailed to this value if storing is not possible. For better comparison of the different nominal FPV power, the dispatched

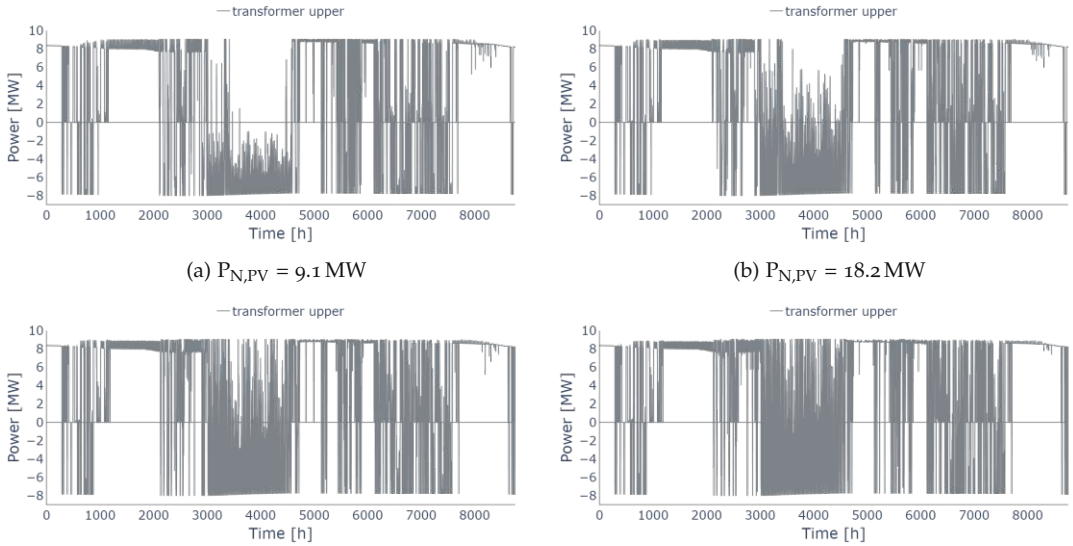

(a) $P_{N,PV}$ = 9.1 MW (b) $P_{N,PV}$ = 18.2 MW

(c) $P_{N,PV}$ = 27.3 MW (d) $P_{N,PV}$ = 36.4 MW

Figure 4.3: Power transfer at the upper grid connection for different values of the nominal FPV power $P_{N,PV}$, without the integration of a BESS

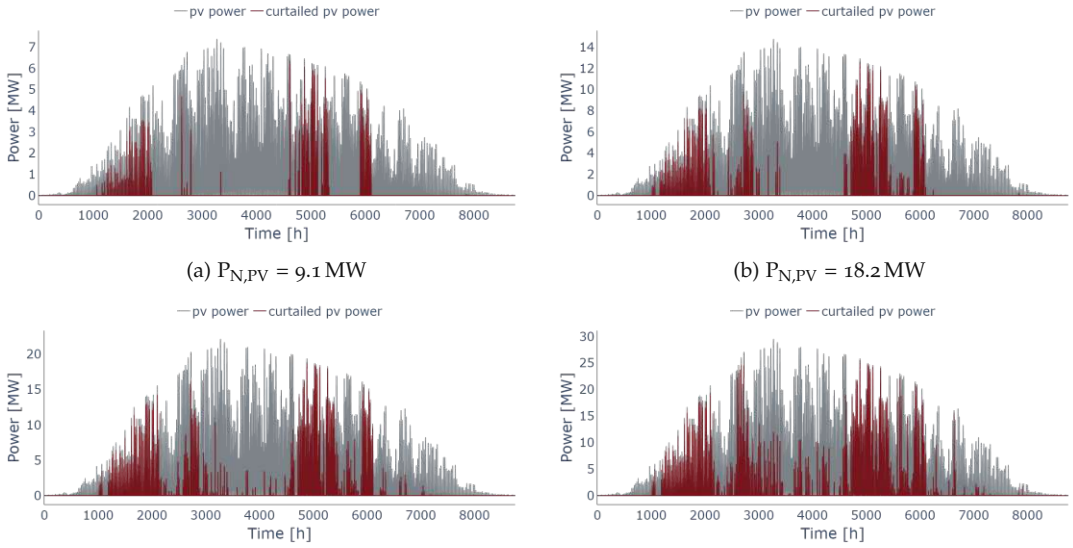

(a) $P_{N,PV}$ = 9.1 MW (b) $P_{N,PV}$ = 18.2 MW

(c) $P_{N,PV}$ = 27.3 MW (d) $P_{N,PV}$ = 36.4 MW

Figure 4.4: Maximum possible power generation profile and curtailed power of the FPV with different nominal power and without the integration of a BESS

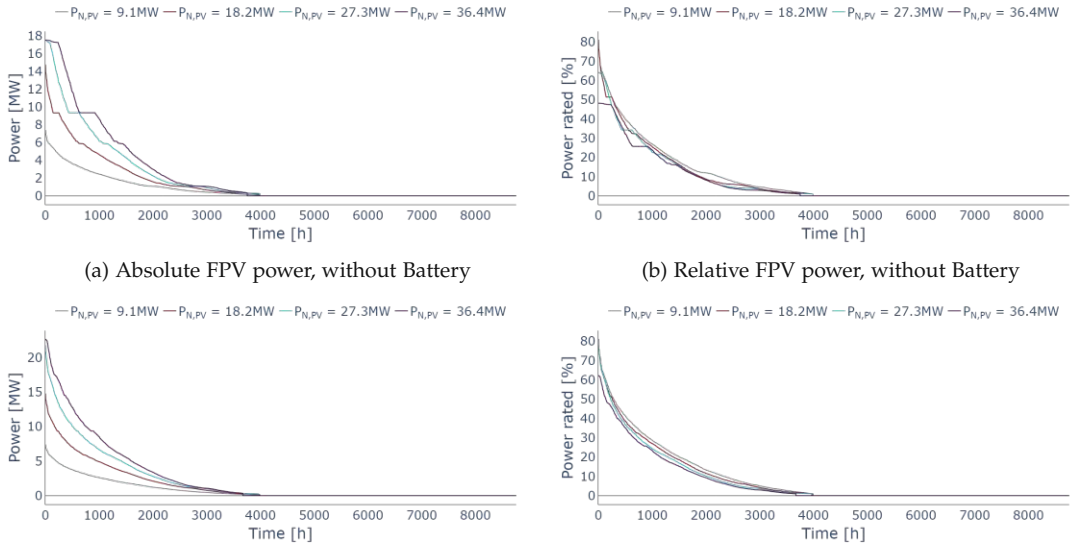

(a) Absolute FPV power, without Battery

(b) Relative FPV power, without Battery

(c) Absolute FPV power, with Battery

(d) Relative FPV power, with Battery

Figure 4.5: Load duration curves for different nominal FPV power, with and without the battery integration (E = 10 MWh, storage duration of 2 h)

FPV power is rated to the nominal power and therefore shown in percentage (Fig. 4.5b). This illustration shows, that the maximum power of the FPV is only 80% and is even curtailed to around 50% for a nominal FPV power of 36.4 MW. With the integration of the BESS, the curtailed power is decreasing as shown in Fig. 4.5c and Fig. 4.5d, and therefore the utilization of the FPV is increased.

As already indicated in Fig. 4.4 and Fig. 4.5 the utilization of the FPV is rather small due to the seasonality of the irradiation and also due to the generally lower maximum energy yield resulting from the lower tilt angle of the modules than for land-based systems. This is illustrated by the full load hours (FLH) of the FPV shown in Fig. 4.6 as heatmaps in dependence of the nominal FPV power and the battery usable storage capacity for a storage duration of 4 and 2 h. The maximum FLH are around 810 h/a for the maximum expansion power of the battery and minimal expansion power of the FPV, while the minimal FLH are around 550 h/a vice versa. Higher FLH can be accomplished by a lower storage duration of the BESS.

As for the FPV integration, the load duration curves of the BESS utilization are also compared for storage durations of 4 h and 2 h and different nominal FPV power levels of 0/18.2/36.4 MW. The most significant difference between the figures is the maximum storage power for the different storage durations, which is due to the resulting rated power of the BESS converter. This leads to more precise trading on the day-ahead

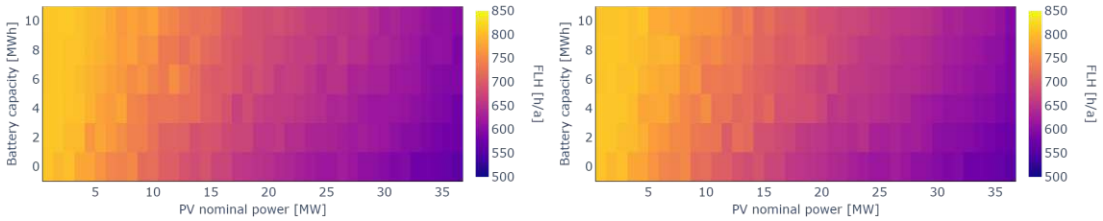

(a) storage duration of 4 h

(b) storage duration of 2 h

Figure 4.6: Full load hours of the FPV for different storage duration and usable energy capacity of the battery and nominal power of the FPV

market, as highs and lows in prices can be used more effectively as the battery is charged or discharged faster with higher power. For increasing nominal FPV power, the utilization of the BESS only increases to a small extent, as most of the FPV's output is used to supply the upper pump.

The effect of increasing nominal FPV power on the annual energy fed into and extracted from the grid is already discussed above. For increasing nominal FPV power the overall feed-in to the grid is increased and the extraction due to the storage is decreased. This influence is illustrated once again in Fig. 4.8c, where the load duration curve is shown for increasing nominal FPV power without a BESS.

In direct comparison Fig. 4.8a and 4.8b depict the influence of the increase of only BESS usable energy capacity with a storage duration of 4 h respectively 2 h. The different influences on the load duration curve can be split up into four different parts:

- In the first part of the load duration curve, the power fed into the grid is increased by synchronous operation of both discharging the BESS and turbining. In these cases, the PSHP can operate without being limited by the operation strategy.
- Around the 4500th hour, the power supplied is decreased on the left-hand side due to charging the battery and increased from zero on the right-hand side due to discharging the battery. This is because of the limited operation of the upper stage due to the operation strategy which limits the economic possibilities. As the final state of the BESS after the optimization horizon is constantly 50% and it can be charged and discharged multiple times in this timeframe, the battery can operate freely.
- Around the 6000th hour the contrary of the above is done. On the left-hand side the extracted power is increased from zero by charging the battery and on the right-hand side is decreased by charging the battery. This again is done asynchronously to the operation of the PSHP as the PSHP is limited by the final storage volume. This leads to a reduction in the economic operation of the PSHP.

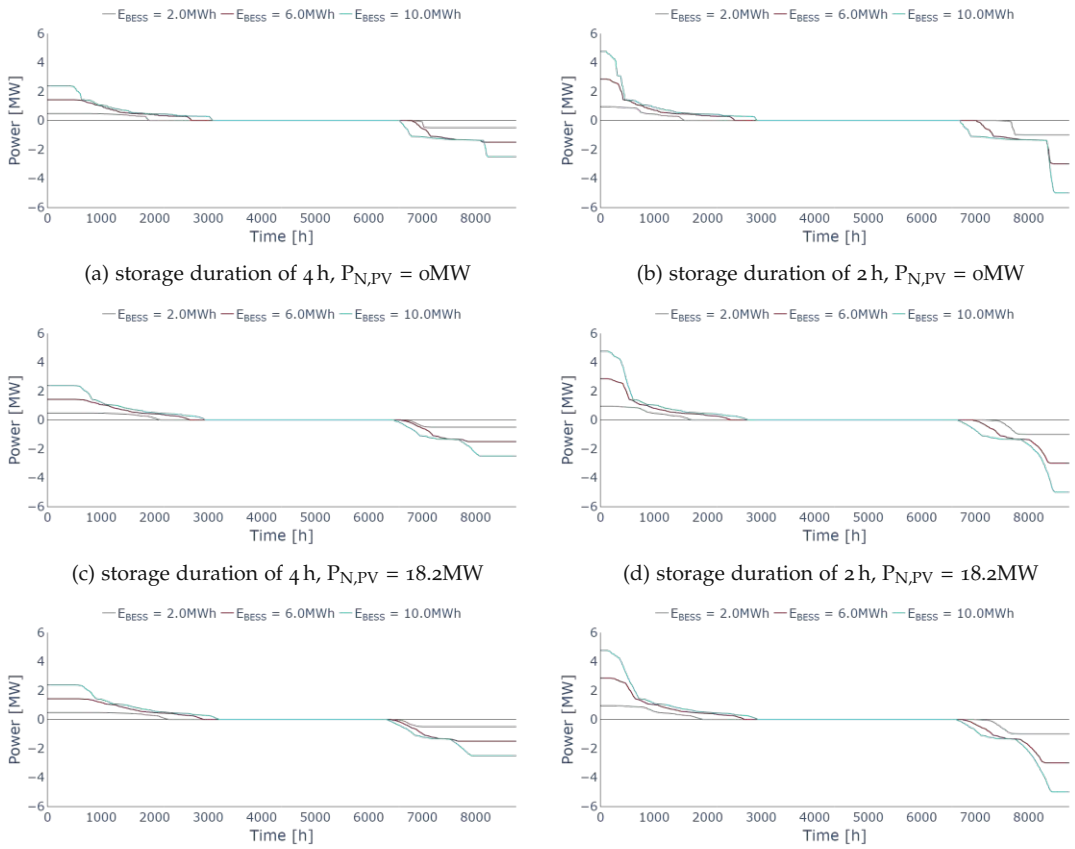

(a) storage duration of 4 h, $P_{N,PV}$ = 0MW

(b) storage duration of 2 h, $P_{N,PV}$ = 0MW

(c) storage duration of 4 h, $P_{N,PV}$ = 18.2MW

(d) storage duration of 2 h, $P_{N,PV}$ = 18.2MW

(e) storage duration of 4 h, $P_{N,PV}$ = 36.4MW

(f) storage duration of 2 h, $P_{N,PV}$ = 36.4MW

Figure 4.7: Sorted battery power for different storage duration and nominal power of the FPV

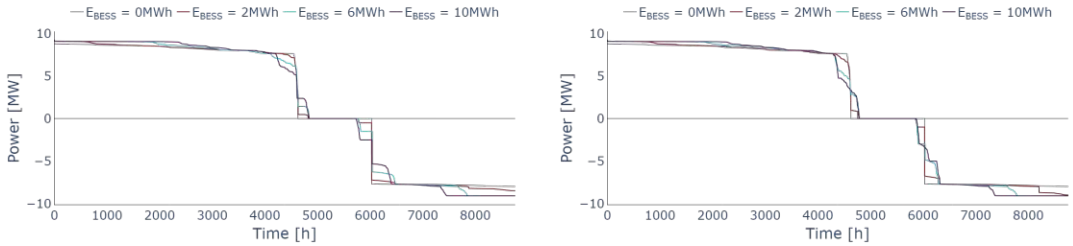

(a) Varying BESS usable energy capacity with BESS storage duration of 4 h and no FPV

(b) Varying BESS usable energy capacity with BESS storage duration of 2 h and no FPV

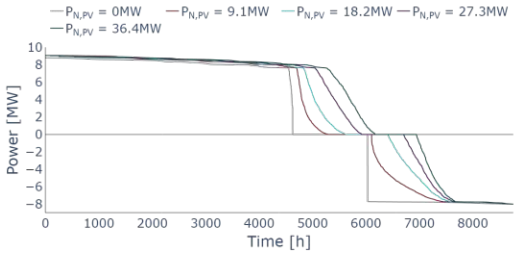

(c) Varying nominal FPV power without a BESS

Figure 4.8: Load duration curve of grid transfer at the upper grid connection for varying nominal FPV power and BESS usable energy capacity (with storage duration of 4 respectively 2 h)

- On the last part of the load duration curve, the extracted power from the grid is increased by the synchronous operation of both the PSHP and the BESS. In contrast to the first part, the delta between the load duration curve with and without the BESS is higher, as it is distributed to a smaller period.

This shows that the technical difference between the operation of the BESS and the PSHP is only due to the limited possible application, caused by the annual progression of the upper reservoir. Without this limitation, the BESS would therefore act in the same manner as the PSHP. With the methods applied in this thesis, the only technical benefit of the BESS therefore is the higher efficiency compared to the round trip efficiency of the PSHP.

In all three subfigures of Fig.4.8 a difference between the total sum of feed-in to the grid and extraction from the grid can be observed. This can be explained by the natural inflow to the upper reservoir. This inflow was to date used to operate the storage power plant, which is taken as a reference for this thesis. The utilization of the turbines can therefore be increased by also including storage pumps.

A combined implementation of both FPV and BESS would lead to a combination of the behavior discussed above for Fig. 4.8. The cumulative annual grid interaction of the entire HPP regarding the extraction and feed-in is shown in the heatmaps of Fig. 4.9,

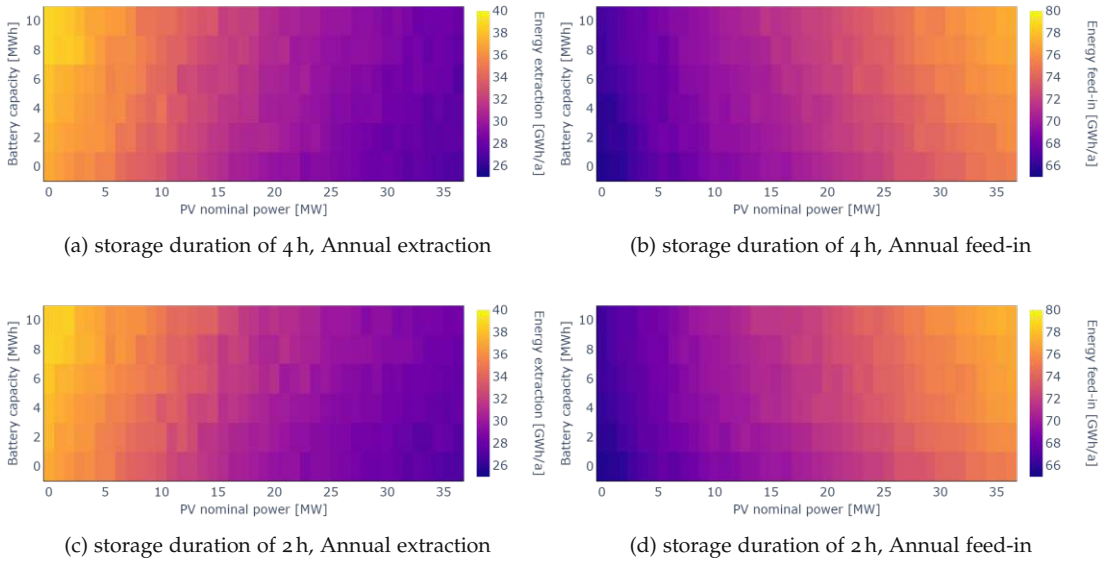

(a) storage duration of 4 h, Annual extraction

(b) storage duration of 4 h, Annual feed-in

(c) storage duration of 2 h, Annual extraction

(d) storage duration of 2 h, Annual feed-in

Figure 4.9: Annual extracted (a, c) and fed-in (b, d) energy to the grid from the hybrid power plant

where the influence of the nominal FPV power and battery usable energy capacity are shown for the two different storage durations of 4 and 2 h. The influence of the storage duration is comparably low as the battery has a very high stand-by time as depicted in Fig. 4.7. The overall energy sums charged into the battery are comparable for both storage durations. The higher extraction and feed-in for a higher battery usable energy capacity is mostly due to arbitrage at the day-ahead market, while also additional FPV generation can be stored which would otherwise be curtailed. The FPV decreases the overall extraction and increases the overall feed-in as it adds more generation, which can also be used to drive the storage pump.

4.2 Economic evaluation

The economic evaluation is performed based on both the LCOE and NPV, which are calculated with equations (3.21) and (3.22) for different sizes of the BESS and FPV simulated in the parameter study. The LCOE only show the levelized costs of each sold energy unit and do not indicate whether the system is economically viable. Therefore, the NPV shows the economic viability which is given for a NPV greater than zero.

The LCOE of the whole HPP are depicted in heatmaps depending on the nominal FPV power and the battery's usable energy capacity shown in Fig. 4.10. Two different WACC

are assumed for the calculations with 6% and 10% [17]. Again, a BESS with a storage duration of 4 h respectively 2 h are assumed. Various influences on the parameters can be derived from these figures, which are listed below:

- The most prominent difference is drawn by comparing the heatmaps with different WACC, where a higher WACC results in higher LCOE. While the LCOE for a WACC of 6% range between 55 EUR/MWh and 100 EUR/MWh, they are between 75 EUR/MWh and 125 EUR/MWh for the higher WACC of 10%. This is due to the higher annuities of the investment costs that have to be taken into account for the whole lifetime.
- By comparing the lower storage duration of 2 h to the higher one of 4 h, the LCOE for increasing BESS usable energy capacity are varying less, and therefore a lower storage duration is more economical. As already stated, this is due to the higher ability to charge the battery in times of low energy prices and therefore decreasing electricity costs. This benefit predominates against the increasing CAPEX and therefore also OPEX of the BESS due to the lower storage duration.
- The LCOE are increasing in the direction of higher battery usable energy capacity as the alternative storage to the PSHP is more expensive regarding its specific CAPEX and the benefits considered in this thesis are rather small.
- The LCOE are increasing in the direction of higher nominal FPV power, where ultimately there are two reasons for this. The curtailed energy is increasing for higher nominal FPV power, which was already discussed above. But even without curtailment, the LCOE of the FPV are higher than the ones of the PSP. Even a higher battery usable energy capacity does not reduce the FPVs LCOE enough. This can be seen in the heatmaps in Fig. 4.11, again depending on the nominal FPV power and the battery usable energy capacity for different WACC and storage duration like in the figures described inhere.

To determine whether the entire system is economically viable, the NPV is calculated. Like for the LCOE, the NPV is again compared for different sizes of the components and the two WACC in the heatmaps shown in Fig. 4.12. The green parts refer to a positive NPV and therefore indicate the economic viability as the revenues throughout the lifetime of the system exceed the expenditures. Red parts are referring to a negative NPV and therefore the system would not be economically viable, based on the assumptions. The yellow parts are associated with a NPV of zero and therefore are the border between the viability and non-viability of the system. The effect of the system parameters on the NPV are again listed below:

- A higher WACC results in lower economic viability of the entire system and reduces the maximum nominal FPV power and battery usable energy capacity, at which it is still evaluated positively regarding the NPV.

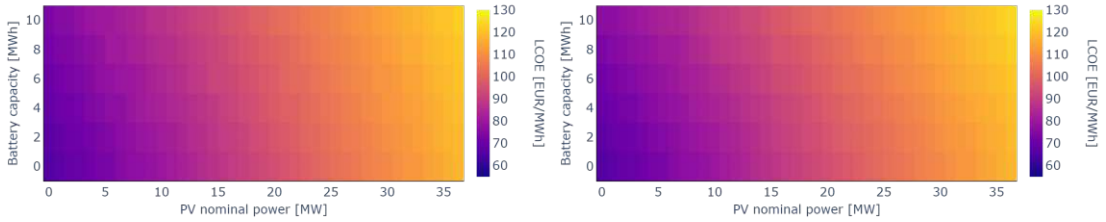

(a) storage duration of 4 h, WACC = 10%

(b) storage duration of 2 h, WACC = 10%

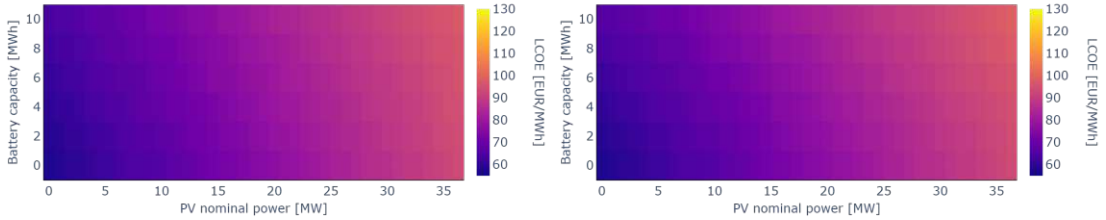

(c) storage duration of 4 h, WACC = 6%

(d) storage duration of 2 h, WACC = 6%

Figure 4.10: LCOE of the total HPP for varying battery usable energy capacity, BESS storage duration, nominal FPV power and WACC

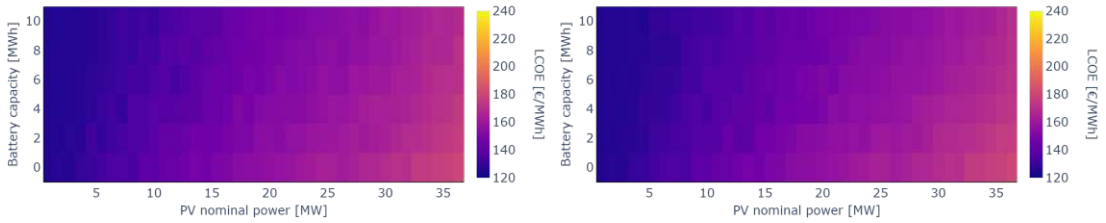

(a) storage duration of 4 h, WACC = 6%

(b) storage duration of 2 h, WACC = 6%

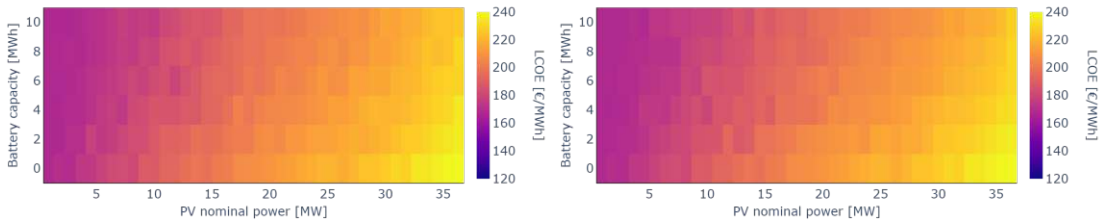

(c) storage duration of 4 h, WACC = 10%

(d) storage duration of 2 h, WACC = 10%

Figure 4.11: LCOE of the FPV for different storage duration and usable energy capacity of the battery, nominal power of the FPV and WACC

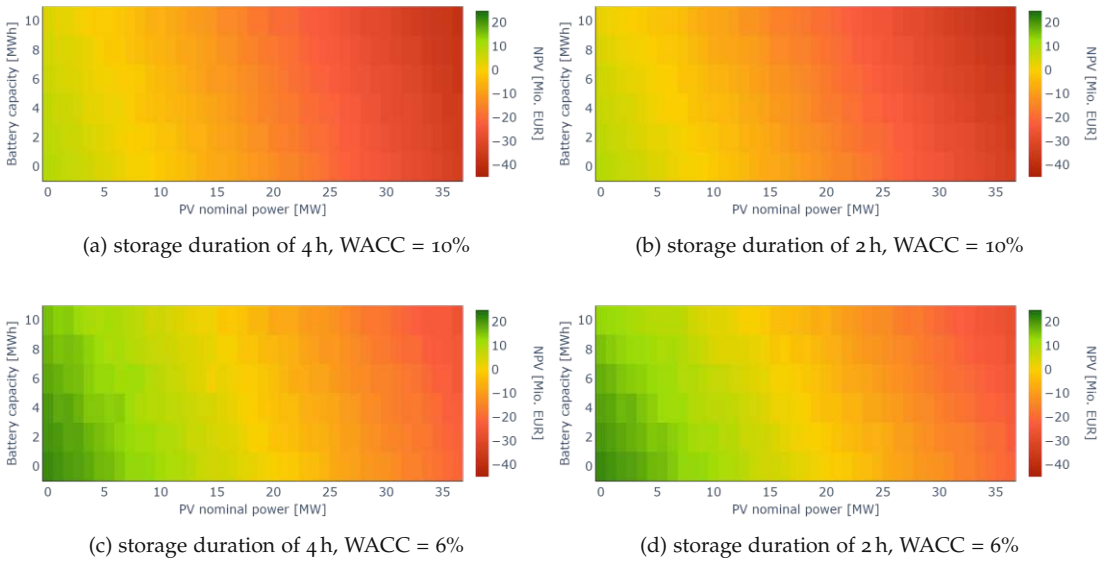

(a) storage duration of 4 h, WACC = 10%

(b) storage duration of 2 h, WACC = 10%

(c) storage duration of 4 h, WACC = 6%

(d) storage duration of 2 h, WACC = 6%

Figure 4.12: NPV of the entire hybrid power plant for varying battery usable energy capacity, battery storage duration, nominal FPV power and WACC

- A lower storage duration makes the NPV less depending on the battery's usable energy capacity, as the benefits resulting from the higher BESS charging/discharging power exceed the higher CAPEX.
- Due to the higher specific CAPEX of the BESS, the NPV decrease for increasing battery usable energy capacity.
- Due to the high CAPEX and the lower utilization for increasing nominal power of the FPV, the NPV of the whole system decreases.

4.3 Impact of the FPV on the evaporation

Based on the given weather data from Meteonorm, the evaporation reduction of the upper reservoir is calculated for a suspended float of the FPV system. For times in which ice is assumed on the reservoir, the evaporation is set to zero. This assumption is based on the snow depth which is also included in the weather data. As in some limited cases the evaporation based on the methodology in Section 3.2.1 is negative, the evaporation is limited to a lower barrier of zero. Reason could be, that the regression model is generated with weather and evaporation data from Italy and therefore cannot be globally used without errors.

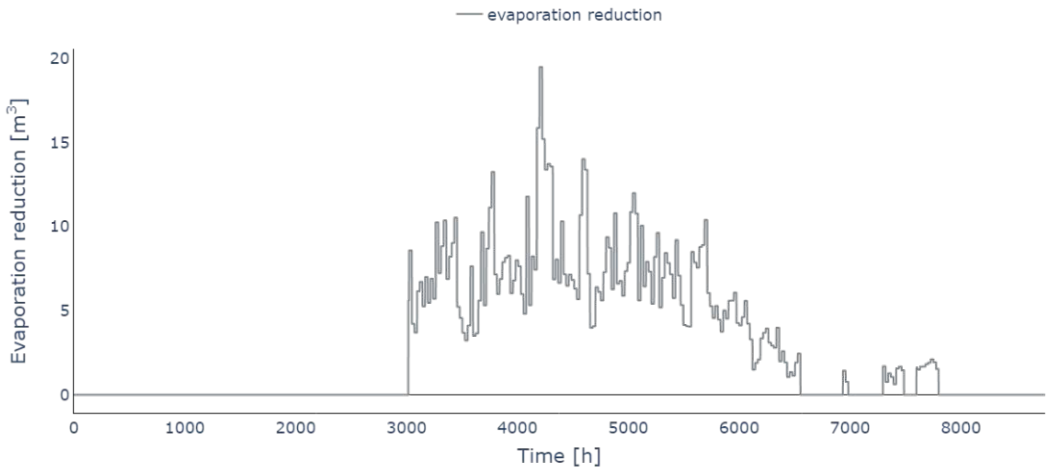

Figure 4.13: Evaporation reduction over the course of one year for an FPV power plant with a nominal power of 9.1MWp

As irradiation and ambient air temperature are highly seasonal, the evaporation is also highest in summer, which therefore leads to the highest evaporation reduction in summer. Depicted in Fig. 4.13 is an exemplary annual evaporation reduction trend for a nominal FPV power of 9.1 MWp. Due to cold temperatures in winter and an ice layer on top of the reservoir the evaporation and therefore also the evaporation reduction is minimal in winter.

The annual sum of the evaporation reduction is increasing linearly with increasing FPV system size. This cumulative evaporation reduction is shown in Fig. 4.14. Even though the amount for a nominal FPV power of 35 MWp with roughly 100.000 m^3 per year seems rather high, it is low compared to the upper storage volume of approximately 61 Mio. m^3. To put this further into reference a volume of 100.000 m^3 leads to 4 h of additional turbining throughout a whole year if a moderate turbining rate of 7 m^3/s is assumed.

4.4 Binary versus ternary operation of the pumped storage power plant

One part of the parameter study is to compare the operation of the pumped storage power plants turbine and pump regarding the combined usage to achieve a variable set point in pumping mode. The optimization model only used both, the pump and the

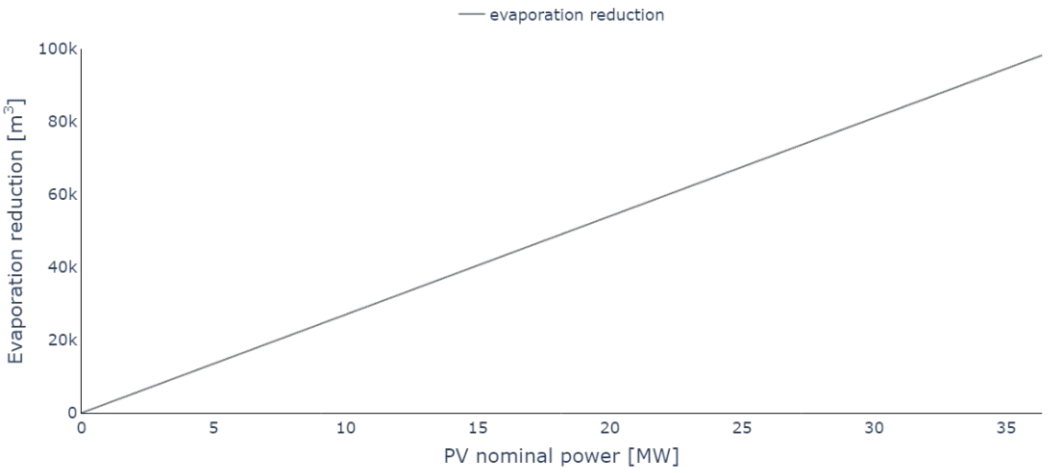

Figure 4.14: Cumulative evaporation reduction of one year for different nominal FPV power

turbine, in the same time step in very few cases, even if ternary operation is possible. This is mostly in summer where the pump did run more or less constantly to achieve the upper reservoir's state of charge, determined by Fig. 3.11, after the optimization horizon of three days. An exemplary utilization of ternary operation is shown in Fig. 4.15 for the base case without FPV and BESS integration. Even though this is a specific case, it shows the overall behavior for the whole parameter study regarding BESS and FPV sizing.

This behavior can be explained by the serial losses of pump, turbine, and generator, which lead to a lower total efficiency of the pump operation and therefore a higher flow compared to binary pumping operation. It is assumed that ternary operation would be utilized more if the PSHP operation portfolio would have a wider spectrum than only trading on the day-ahead market. Another reason could be the simplification of the optimization model to a linear model.

Due to the small differences between the pump and turbine utilization in binary and ternary operation, only the results for binary operation are presented and described in the previous sections of this chapter.

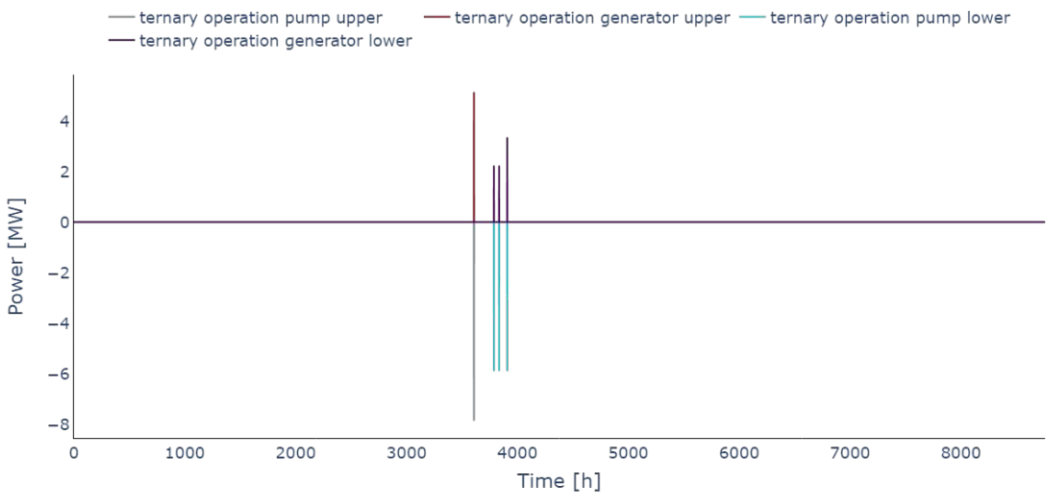

Figure 4.15: Ternary operation of both PSHP stages for the base case without FPV and BESS integration.

5 Conclusion

The FPV increases the LCOE of the HPP with increasing expansion capacity. Also, the NPV decreases with increasing nominal power of the FPV. The reason for the decreasing profitability is, on the one hand, the low energy yield of the FPV, which is due to the low irradiation at the site and the low tilt angle. On the other hand, the LCOE of FPV are generally higher compared to PSHP. Even if the economic efficiency decreases with the higher nominal power of the FPV, the technical advantages are high, as the FPV increases the total feed-in and reduces the total purchase from the grid. The grid connection is therefore better utilized through hybrid operation. The economically viable size of the FPV is up to twice the maximum transferable power, which is made possible by the storage capacity of the PSHP.

The BESS makes it possible to increase the utilization of the FPV, as it provides additional storage capacity for excess FPV generation. Even if the utilization of the FPV is increased, the economic viability decreases as the BESS is a component with high investment costs. Therefore, based on the purely market-driven implementation in the optimization model, the BESS is not recommended for use exclusively on the day-ahead market from an economic perspective. Technical incentives such as an extended lifetime of PSHP components used alternatively for ancillary services could be a useful method for hybridization.

The evaporation reduction at the PSHP site investigated is rather low, even with a high implementation of FPV. Therefore, the evaporation reduction does not have a major impact on the operation of the PSHP. This effect will be greater at another site with higher irradiation and ambient temperature, although the actual effects are not clear and should be studied in future work. Another possible improvement in evaporation reduction is caused by climate change and the resulting increase in temperatures, which will make evaporation an increasingly important issue.

It turns out that ternary operation is not a frequently used option of the optimization model, as the lower efficiency of this pump operation mode leads to higher water losses in the upstream reservoir. The ternary operation could be used more if the PSHP is not only optimized for trading on the day-ahead market but also provides ancillary services such as primary or secondary reserve.

This thesis shows that both the PSHP and the FPV have a seasonality in power generation that enables synergies between the two technologies. The high energy demand of the PSHP can be partially covered by the generation of the FPV. The seasonality of the PSHP is based on the operating strategy of the upper basin, which is implemented due to the excessively long solving time of the optimization model. Therefore, the PSHP has limited flexibility and cannot be operated optimally during periods of high FPV generation. A possible solution could be to implement a second, simplified optimization model that is abstracted from the model used in this work. This simplified optimization model would then be used as the basis for the short-term operating strategy. It is assumed that this increased flexibility would further increase the hybridization potential between the two technologies, as the provoked seasonality of the PSHP partially reduces the utilization of the FPV.

In future work, this method could also be applied to other climate zones to further evaluate the effects of FPV on evaporation. As the reference PSHP is located in central Sweden, the evaporation reduction potential is rather low due to the cold temperatures. The optimization model and thus also the economic evaluation should be adapted for the inclusion of auxiliary services in the HPP's portfolio. The technical advantages of the BESS should also be considered, as it has a positive effect on the degradation of the wearing parts of the PSHP. Finally, studies on the influence of evaporation on the energy yield should be of interest, as changes in the energy yield have an impact on the economic viability of the system.

6 Acknowledgement

I would like to thank everyone who supported, encouraged and challenged me throughout my studies. Above all, I would like to thank my parents, who made my studies possible in the first place, and especially my mother for her encouragement in stressful times. I also owe a big thank you to my partner Carolin Gunz, who has always motivated me and given me strength in stressful phases. I would also like to thank her and Rainer Gunz for proofreading my work and for their valuable suggestions for improvement.

With regard to the TU Vienna, my special thanks go to Prof. Johann Auer and Antonia Golab, who were always a great support to me during the diploma seminars and in bilateral exchanges. I would also like to thank the rest of the team for their input during the diploma seminar.

On the AIT side, I would like to thank Johannes Kathan for the opportunity to write my thesis in the research field of Hybrid Power Plants. Special thanks go to my AIT supervisor Sebastian Steinlechner, who gave me excellent support and challenges during my work. I would also like to thank my office colleagues Christian Messner, Christian Seitl and Fabian Leimgruber as well as Judith Kapeller, Yannick Wimmer, Sebastian Bittner and Klara Maggauer, who were always open to constructive discussions with me and helped me with methodological questions. A big thank you also goes to Stefan Strömer, who invested a lot of time helping me to create the optimization model.

I would also like to thank Thomas Eder, Thomas Sageder and Lorenz Neururer from Global Hydro for the exchange and support as well as for the exceptionally good data. Without this help, the work would never have been possible to this extent.

Finally, I would also like to thank the operators of the reference power plant for their support, who made my work possible through discussions and the provision of data.

Bibliography

[1] IEA, *Net zero by 2050*, IEA, Ed., Paris, 2021. [Online]. Available: https://www.iea.org/reports/net-zero-by-2050 (cit. on p. 1).

[2] World Bank Group, ESMAP and SERIS, Ed., *Where sun meets water: Floating solar market report*, Washington, DC: World Bank, 2019 (cit. on pp. 1, 5–7).

[3] Z. Šimić, D. Topić, G. Knežević, and D. Pelin, "Battery energy storage technologies overview," *International journal of electrical and computer engineering systems*, vol. 12, no. 1, pp. 53–65, 2021, ISSN: 18476996. DOI: 10.32985/ijeces.12.1.6 (cit. on p. 3).

[4] *Electricity storage and renewables: Costs and markets to 2030*. [Abu Dhabi]: International Renewable Energy Agency, 2017, ISBN: 978-92-9260-038-9 (cit. on p. 4).

[5] L. Bahner, A. Schreider, and R. Bucher, "Batteries and pumped-hydro: Pooling for synergies in the frequency response provisioning," in *Proceedings of the 13th International Renewable Energy Storage Conference 2019 (IRES 2019)*, pp. 109–118. [Online]. Available: https://www.atlantis-press.com/article/125923323 (cit. on p. 4).

[6] Verbund, Ed., *Bluebattery: Größte kraftwerks-batterie österreichs in betrieb*, Wallsee-Mitterkirchen, 2020. [Online]. Available: https://www.verbund.com/de-at/ueber-verbund/news-presse/presse/2020/09/17/blue-battery-eroeffnung#!/1/undefined/1/undefined/%7B%22sitepath%22%3A%22d6d95304-b13d-4d4e-8b01-88979d3f49e0%22%2C%22database%22%3A%22web%22%2C%22language%22%3A%22de%22%2C%22token%22%3A%22ipz06ng01trsas2k4odwm%22%2C%22folder%22%3A%22celum%22%2C%22page%22%3A0%2C%22isMobile%22%3Afalse%7D/undefined (visited on 02/19/2024) (cit. on p. 4).

[7] *Floating-pv-anlage in grafenwörth*. [Online]. Available: https://www.ecowind.at/unternehmen/referenzen/floating-pv-anlage-grafenwoerth/ (visited on 03/14/2023) (cit. on p. 5).

[8] L. Micheli, "The temperature of floating photovoltaics: Case studies, models and recent findings," *Solar Energy*, vol. 242, pp. 234–245, 2022, ISSN: 0038092X. DOI: 10.1016/j.solener.2022.06.039 (cit. on pp. 6, 29).

[9] M. Kumar, H. Mohammed Niyaz, and R. Gupta, "Challenges and opportunities towards the development of floating photovoltaic systems," *Solar Energy Materials and Solar Cells*, vol. 233, p. 111 408, 2021, ISSN: 09270248. DOI: 10.1016/j.solmat.2021.111408 (cit. on pp. 6, 29).

[10] F. Bontempo Scavo, G. M. Tina, A. Gagliano, and S. Nižetić, "An assessment study of evaporation rate models on a water basin with floating photovoltaic plants," *International Journal of Energy Research*, vol. 45, no. 1, pp. 167–188, 2021, ISSN: 0363-907X. DOI: 10.1002/er.5170 (cit. on pp. 7, 14–16).

[11] A. Barbón, Á. Gutiérrez, L. Bayón, C. Bayón-Cueli, and J. Aparicio-Bermejo, "Economic analysis of a pumped hydroelectric storage-integrated floating pv system in the day-ahead iberian electricity market," *Energies*, vol. 16, no. 4, p. 1705, 2023. DOI: 10.3390/en16041705 (cit. on pp. 7, 8).

[12] G. Kakoulaki, R. Gonzalez Sanchez, A. Gracia Amillo, *et al.*, "Benefits of pairing floating solar photovoltaics with hydropower reservoirs in europe," *Renewable and Sustainable Energy Reviews*, vol. 171, p. 112 989, 2023, ISSN: 13640321. DOI: 10.1016/j.rser.2022.112989 (cit. on p. 8).

[13] N. Lee, U. Grunwald, E. Rosenlieb, *et al.*, "Hybrid floating solar photovoltaics-hydropower systems: Benefits and global assessment of technical potential," *Renewable Energy*, vol. 162, pp. 1415–1427, 2020, ISSN: 09601481. DOI: 10.1016/j.renene.2020.08.080 (cit. on p. 8).

[14] L. Liu, Q. Sun, H. Li, H. Yin, X. Ren, and R. Wennersten, "Evaluating the benefits of integrating floating photovoltaic and pumped storage power system," *Energy Conversion and Management*, vol. 194, pp. 173–185, 2019, ISSN: 01968904. DOI: 10.1016/j.enconman.2019.04.071 (cit. on p. 8).

[15] Pöyry Energy AG, *Bestimmung von wirkungsgraden bei pumpspeicherung in wasserkraftanlagen*, 2008 (cit. on pp. 16, 20, 27).

[16] Ankit Rohatgi, *Webplotdigitizer - web based plot digitizer*. [Online]. Available: https://apps.automeris.io/wpd/ (visited on 02/03/2024) (cit. on pp. 18, 21).

[17] *Where sun meets water: Floating solar handbook for practitioners.* Washington, DC: World Bank, 2019. (visited on 02/09/2024) (cit. on pp. 28, 29, 42).

[18] *Water reservoirs and hydro storage plants: Aggregate filling rate of water reservoirs and hydro storage plants [16.1.d]*. [Online]. Available: https://transparency.entsoe.eu/generation/r2/waterReservoirsAndHydroStoragePlants/show (visited on 02/09/2024) (cit. on pp. 28, 29).

[19] W. F. Holmgren, C. W. Hansen, and M. A. Mikofski, "Pvlib python: A python package for modeling solar energy systems," *Journal of Open Source Software*, vol. 3, no. 29, p. 884, 2018. DOI: 10.21105/joss.00884 (cit. on p. 28).

[20] M. Dörenkämper, A. Wahed, A. Kumar, M. de Jong, J. Kroon, and T. Reindl, "The cooling effect of floating pv in two different climate zones: A comparison of field test data from the netherlands and singapore," *Solar Energy*, vol. 214, pp. 239–247, 2021, ISSN: 0038092X. DOI: 10.1016/j.solener.2020.11.029 (cit. on p. 29).

[21] *Day-ahead prices: Day-ahead prices [12.1.d]*. [Online]. Available: https://transparency.entsoe.eu/transmission-domain/r2/dayAheadPrices/show (visited on 02/14/2024) (cit. on p. 30).

[22] Svenska Kraftnät, Ed., *Prislista 2022 för transmissionsnätet*, 2022. [Online]. Available: https://www.svk.se/en/stakeholders-portal/electricity-market/connecting-to-the-grid/tariffcharges/#:~:text=The%20grid%20tariff%20is%20a,the%20actual%20input%20takes%20place. (visited on 10/06/2023) (cit. on p. 30).

[23] V. Ramasamy and R. Margolis, *Floating photovoltaic system cost benchmark: Q1 2021 installations on artificial water bodies*, National Renewable Energy Laboratory, Ed., Golden, CO, Oct. 2021. [Online]. Available: https://www.nrel.gov/docs/fy22osti/80695.pdf (visited on 02/14/2024) (cit. on p. 31).

[24] *Utility-scale battery storage*, 2023. [Online]. Available: https://atb.nrel.gov/electricity/2023/utility-scale_battery_storage (visited on 02/14/2024) (cit. on p. 31).